Ore Geology Reviews 89 (2017) 171–186

Contents lists available at ScienceDirect

Ore Geology Reviews

journal homepage: www.elsevier.com/locate/oregeo

The Chalukou deposit in the North Great Xing'an Range of China: A protracted porphyry Mo ore-forming system in a long-lived magmatic evolution cycle

Yifei Liu [a,*], Leon Bagas [a,b], Sihong Jiang [a], Fengxiang Wang [a]

[a] MLR Key Laboratory of Metallogeny and Mineral Assessment, Institute of Mineral Resources, Chinese Academy of Geological Sciences, Beijing 100037, China
[b] Centre for Exploration Targeting, University of Western Australia, 35 Stirling Highway, Crawley WA 6009, Australia

ARTICLE INFO

Article history:
Received 1 July 2016
Accepted 25 April 2017
Available online 21 June 2017

Keywords:
Porphyry Mo deposit
Multiphase intrusion
Protracted ore-forming system
North Great Xing'an Range
Xing'an-Mongolia Orogen

ABSTRACT

The Chalukou deposit is located in the North Great Xing'an Range of the Xing'an-Mongolia Orogen bordering and to the northeast of the North China Craton. The deposit is a high-F-type porphyry Mo deposit hosted by the Chalukou composite igneous body containing small intrusive bodies genetically related to Mo mineralization. The composite igneous body includes pre-mineralization dolerite, monzogranite and syenogranite, syn-mineralization rhyolitic porphyry, granitic porphyry and fine-grained monzogranite, and post-mineralization rhyolitic porphyry, quartz porphyry, dioritic porphyry and andesitic porphyry. Detailed laser ablation inductively coupled plasma mass spectrometry (LA-ICP-MS) U-Pb zircon dating of the igneous components of the composite igneous body was carried out to determine the temporal framework for magmatism in the Chalukou region. The new LA-ICP-MS U-Pb ages constraint documented here, together with the published ages, indicate that there was a protracted porphyry Mo ore-forming event of approximately 7 million years between ca. 152 when the ore related rhyolitic porphyry was emplaced and ca.145 Ma when molybdenite ceased being deposited. The dating reveals that the mineralization is a part of relatively long-lived magmatic cycle involving the emplacement of small doleritic stocks at ca. 165 Ma that progressively evolved into extensive granitic intrusions at ca. 164 Ma, and then diminished with the emplacement of mineralization-related porphyries to ca. 152 Ma. The emplacement of barren Early Cretaceous magmatism, represented by volcanic units in the ca. 136 Ma Guanghua Formation and porphyries, followed the mineralized magmatism.

The syn-mineralization porphyry units associated with Mo contain zircons assaying ~15 times higher in U and Th than the pre-mineralization magmatic phases. This indicates that there was a significant enrichment of Mo, U and Th in the magma, and directly associated with ore fluid exsolution. The return to their normal levels in the three elements in the post-mineralization magmatic phases indicates that they were exhausted from the magma chamber in the later phases. A genetic model is proposed for the enormous introduction of ore metals and enrichment at the Chalukou deposit. The protracted and multiphase igneous activity during the long-lived magmatism reflects a multistage enrichment of metal, and may play a crucial role in the formation of a volatile-enriched, fertile and large-volume magma chamber beneath the Chalukou deposit. Such a chamber is envisaged to be required for the formation of porphyry Mo deposits in general.

1. Introduction

Porphyry Mo deposits with Mo/Cu ratios >1 are a major source for Mo and represent an end-members of porphyry Cu-Mo-Au-Sn-W deposits. Several decades of investigation by various groups have shown that these deposits are found in extensional tectonic settings, are genetically associated with small volumes of highly differentiated and evolved magma, and formed after peak magmatic activities (e.g. Westra and Keith, 1981; Schönwandt and Petersen, 1983; Carten et al., 1988; Bookstrom, 1989; Lowenstern et al., 1993; McCandless and Ruiz, 1993; Brooks et al., 2004; Ludington, 2009; Audetat, 2010; Audetat et al., 2011; Chapin, 2012). Recent studies indicate that large volumes of melt are required to form an economic porphyry Mo deposit (Keith et al.,

* Corresponding author at: 26 Baiwanzhuang Street, Xicheng, Beijing 100037, China.
E-mail address: lyfsky@126.com (Y. Liu).

http://dx.doi.org/10.1016/j.oregeorev.2017.04.035
0169-1368/

1986; Cline and Bodnar, 1991; Lowenstern, 1994; Shinohara et al., 1995; Klemm et al., 2008; Audetat, 2010). Furthermore, many porphyry deposits are related to a multiphase magmatic evolution and a protracted ore-forming history (Villeneuve et al., 2001; Ballard et al., 2001; Halter et al., 2002; Barra et al., 2003, 2005; Harris et al., 2008; Feely et al., 2010; Sillitoe and Mortensen, 2010; Quadt, 2011; Liu et al., 2012; Gardien et al., 2016). Despite the close association of highly differentiated small magmatic stocks with porphyry Mo deposits, a number of uncertainties remain. It is not always clear whether these stocks represent isolated mineralization-related magmatic events or are outcomes of long-lived magmatic events. In addition, the initiation and duration of porphyry mineralizing events are not always exactly understood (Quadt, 2011). Therefore, a detailed study of the magmatic evolution of these deposits provides an opportunity to better understand the evolution of ore-forming magma and will help to reveal the role that multiphase intrusions plays in the introduction and enrichment of metals in porphyry Mo deposits.

A number of economic mineral discoveries have been made in the North Great Xing'an Range during the 1950s and most being porphyry copper, hydrothermal Pb-Zn-Ag veins and orogenic Au deposits. These deposits include the Duobaoshan porphyry Cu-Mo (Cui et al., 2008; Zhao et al., 1997), Wunugetushan porphyry Cu-Mo (Qin et al., 1999; Chen et al., 2011), Jiawula-Chaganbulagen Pb-Zn-Ag vein (Xie and Liu, 2001), Eren Tolgoi Ag vein (Lü et al., 2000), and Shabaosi orogenic Au (Wu et al., 2006) deposits. The Chalukou Mo deposit is located at 123°52′E, 51°10′N, and was discovered in 2006 during a follow-up exploration program completed by the No. 706 Geological Party of the Heilongjiang Non-Ferrous Metal Geological Exploration Bureau following the detection of a high-grade Zn-Pb-Ag-Mo stream-sediment anomaly. The results of subsequent detailed drilling between 2007 and 2013 have been used to outline a resource of >2000 Mt grading 0.09% Mo.

The Chalukou deposit has attracted a great deal of attention from researchers since its discovery. The features of the deposit investigated are: (1) its geology and mineralization style (Lü et al., 2010; Fu et al., 2011; Wang et al., 2011; Jin et al., 2014, 2015); (2) the ages of granites in the deposit (Liu et al., 2013a, 2014a; Li et al., 2014; Zhang and Li, 2017); (3) the mineralization age (Nie et al., 2011; Liu et al., 2014a); (4) the geochemistry of granites associated with the deposit (Nie and Jiang, 2011; Liu et al., 2015; Li et al., 2014); (5) the geochemistry of sulfides (Liu et al., 2014b; Hu et al., 2014; Jin et al., 2015); (6) the evolution of hydrothermal fluid based on fluid inclusion studies (Liu et al., 2014b; Xiong et al., 2014); and (7) and the tectonic setting during the formation of the deposit (Liu et al., 2011; Li et al., 2014; Liu et al., 2014a, 2015; Hu et al., 2014). Various studies indicate that Chalukou is a high-F Mo deposit formed during a Mesozoic extensional tectonic setting related to highly evolved granitic magma (Liu et al., 2011, 2014; Jin et al., 2014). Although much work was done on the deposit, there are still some significant and unanswered questions about why so much Mo has been concentrated in a small area. In this manuscript, we focus on the role of multiphase and protracted magmatic evolution history during the ore formation using LA-ICP-MS U-Pb zircon geochronology. In addition, combined with concentration of U and Th in zircons and published ages, we propose that a protracted magmatic-hydrothermal event in a long-lived magmatic evolution are favourable criteria for the introduction and enrichment of a large volume of metals in a volatile-enriched, fertile and large-volume magma chamber that is envisaged to be present beneath the Chalukou Mo deposit. We suggest that the concentration of Th and U in zircons is a useful tool to discriminate which magmatic phase in a multiphase granite is directly related to Mo mineralization.

2. Regional geology

The Chalukou deposit is located in the North Great Xing'an Range and in the Xing'an-Mongolia Orogen (XMO) of northeastern China (Fig. 1b, Jahn et al., 2001; Meng, 2003; Xiao et al., 2003; Xu et al., 2014, 2015; Pirajno and Zhou, 2015). The tectonic activities in the Chalukou region involve the effects of Paleozoic subduction of the Paleo-Asian Oceanic Plate beneath the Siberia and North China cratons, collision of the cratons during the end of the Paleozoic, and a post-orogenic extension and tectonothermal event during the Mesozoic (Jahn et al., 2001; Meng, 2003; Wu et al., 2011; Pirajno and Zhou, 2015). The region may have also been affected by the closure of the Mongol–Okhotsk Ocean and subduction of the Paleo-Pacific Ocean during the Mesozoic (Wu et al., 1999; Tomurtogoo et al., 2005; Guo et al., 2010; Wu et al., 2011, 2013). Under this tectonic regime, a prominent NE-trending structural fabric developed in the region forming basins, folds, crustal-scale faults, and the distribution of major igneous intrusions.

The oldest rocks in the northern part of the XMO are assigned to the Precambrian Xinghuadukou Group, which is composed of migmatite, granulite, biotite-plagioclase gneiss, augen orthogneiss, staurolite garnet two-mica schist and marble, and constitutes the Precambrian crystalline basement in the region. Zircons from the group yield a series of U-Pb ages ranging from the Paleoproterozoic to Neoproterozoic (Zhou et al., 2011; Wu et al., 2012; Sun et al., 2013; Xu et al., 2015).

The Xinghuadukou Group is unconformably overlain by the Neoproterozoic to Cambrian Luomahu, Zhalantun and Wolegen groups consisting of a series of rocks with low metamorphic grades (Miao et al., 2007; Liu et al., 2015; Zhang and Li, 2017). Early Palaeozoic volcanic-sedimentary sequences are extensive in the region and include the Early Ordovician Duobaoshan and Tongshan calc-alkali volcanic formations with an interpreted arc affinity that host the Duobaoshan and Tongshan porphyry Cu deposits (Wu et al., 2015). Devonian and Early Carboniferous volcanic-sedimentary sequences composed of marine volcanic-sedimentary rocks, including sandstone and shale, flysch deposits, layered phases of silica, keratophyre, and calc-alkali and alkali volcanics unconformably overlie these formations. The overlying Late Carboniferous to Permian rocks are marine terrigenous clastic and volcanic rocks (Zhao et al., 2010; Yang et al., 2011). Mesozoic volcanic rocks are widespread in the northern part of the Great Xing'an Range, and have a wide range of compositions ranging from basaltic andesite, trachyandesite and trachydacite to rhyolite, and most of exhibit have a high-K calc-alkaline affinity, and are believed to have been formed during decompressional partial melting in an extensional regime (Ying et al., 2010; Xu et al., 2013).

Widespread Phanerozoic intermediate to felsic intrusions characterize the northern part of the XMO (Wu et al., 2011). Early Paleozoic granitic intrusions related to subduction of the Paleo-Asian Ocean are the oldest present in the area, and some are genetically related to porphyry Cu mineralization, such as the Duobaoshan Cu deposit (Ge et al., 2007; Cui et al., 2008; Wu et al., 2011). Late Paleozoic intrusions are relatively minor, but Mesozoic magmatic rocks are extensive and most are granitic, which include Early Jurassic magmatic-arc granites related to the south to eastward subduction of the Mongolian-Okhotsk Ocean in the west part of the North Great Xing'an Range, and highly fractionated granites formed in an extensional tectonic setting (Wu et al., 1999, 2002, 2003a,b, 2011; Jahn et al., 2001; Lin et al., 2004; Ge et al., 2005). Several polymetallic hydrothermal deposits in the region have a temporal and spatial relationship with the highly fractionated Mesozoic granites.

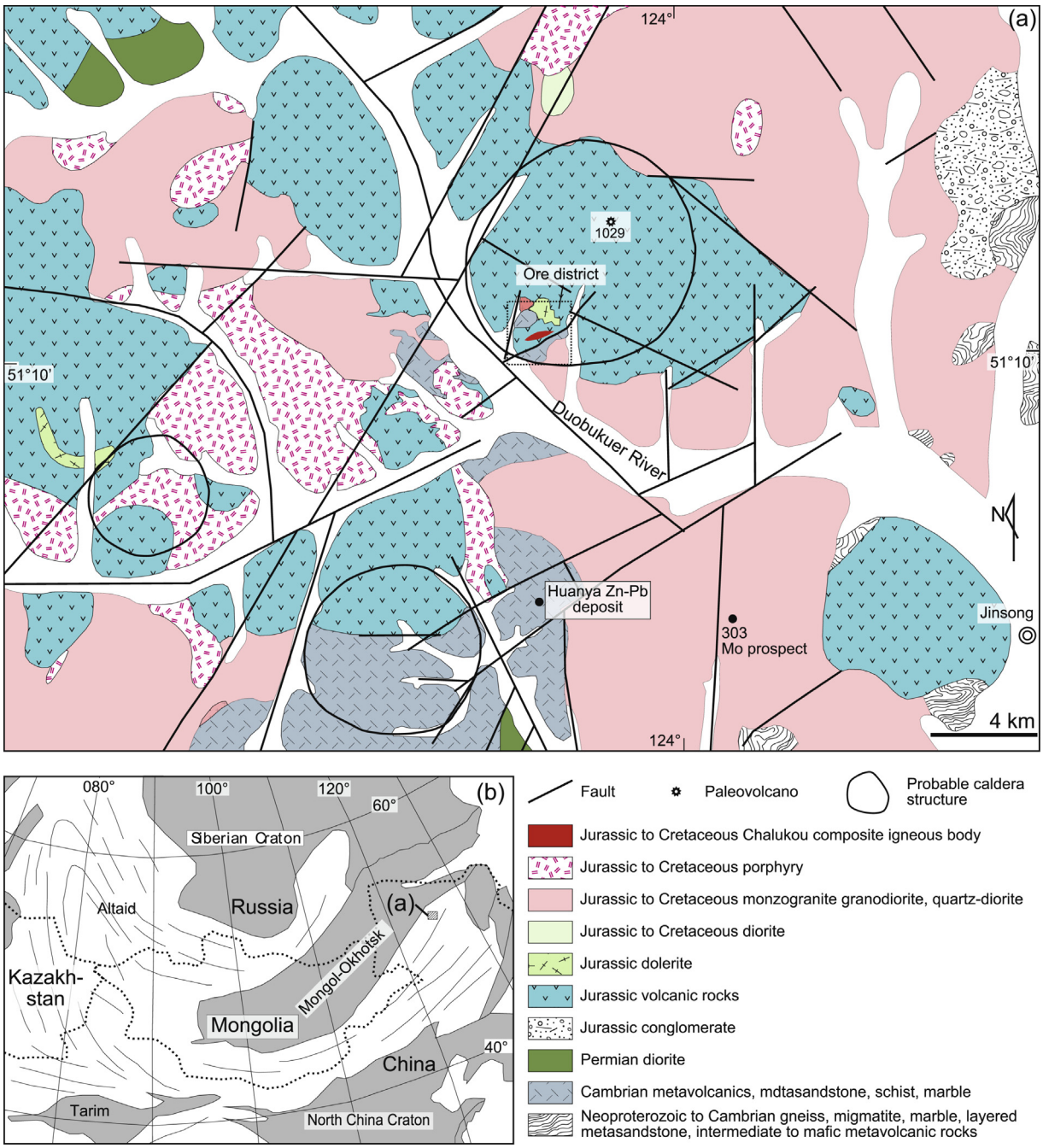

Fig. 1. Chalukou: (a) geological map showing the main rock types and faults with volcanic edifices (modified after JMIC, 2011); and (b) tectonic scheme of the eastern segment of the Central Asian Orogen showing the location and geological setting (modified after Jahn et al., 2000).

3. Local geology

Units exposed in the Chalukou region include a variety of Precambrian to Mesozoic igneous, sedimentary, and metamorphic rocks. The predominant units are in the Precambrian amphibolite facies Xinhuadukou Group, low-grade Cambrian Wolegen Group, Carboniferous sedimentary sequences, and Cretaceous volcanics. The Xinhuadukou Group consists of gneiss, migmatite, marble, laminated meta-sandstone and mafic to intermediate meta-volcanic rocks (Miao et al., 2007; Zhou et al., 2011). The Wolegen Group unconformably overlies the Xinhuadukou Group in the Chalukou region, and consists of marine marble, schist, quartzite, metabasalt, and intermediate porphyries. The Carboniferous sedimentary succession unconformably overlies the Wolegen Group and consists of bioclastic limestone, sandstone, and shale deposited in an arc tectonic setting (Zhao et al., 2012; Yang et al., 2011). The widespread Late Jurassic-Early Cretaceous volcanic sequences consist of felsic tuff, lava, volcaniclastic rocks, and basalt in the Baiyingaolao and Guanghua formations, which were deposited in an extensional tectonic setting (Shao et al., 1999; Ge et al., 2000; Lin et al., 2004; Zhang et al., 2007).

3.1. Intrusive rocks

Extensive volcanic edifices with well-developed annular and radial faults characterize the Mesozoic magmatism in the Chalu-

kou region. Multiphase intrusions of subvolcanic stocks and Mo-Pb-Zn-Ag mineralization in the district are most likely due to the long-lived activity of a Late Jurassic paleovolcano locally known as "1029" (Fig. 1). The location of the Mesozoic Chalukou composite igneous body is structurally controlled by NE-trending faults in the southern part of the region (Fig. 1). Other faults trend NW, SN and eastward (Fig. 1).

The Chalukou Mo mineralization is polymetallic containing elevated Pb-Zn-Ag in the upper part of the deposit. The deposit is located on the northeastern side of the Duobukuer River and the southwest flank of the "1029" paleovolcano (Fig. 1), and is associated with a suite of porphyritic intrusions that form a >1000 m long and 200 m igneous and complex that is at least 1000 m deep. Late Jurassic to Early Cretaceous granites, volcanic rocks and porphyries in the composite igneous body define a sequence of magmatic events associated with Mo and base metal mineralization (Figs. 2, 3). The sequence starts with doleritic dykes followed by a medium-grained pre-mineralization biotite monzogranite succeeded by severely altered stocks related to Mo-Zn-Pb-Ag mineralization, followed by the extensive eruption of the volcanic rocks included in the Early Cretaceous Guanghua Formation, and finally the emplacement of post-mineralization dioritic, andesitic and quartz porphyries. The pre-mineralization granite is covered by the Early Cretaceous volcanic rocks in the central part of the deposit and only crops out to the north and south of the deposit (Fig 1). The result of diamond-drilling shows that the biotite monzogranite borders part of the deposit where it is intensely silicified containing variable proportions of sericite, argillite, and fluorite as alteration products at depth.

The Chalukou composite igneous body is pipe-like in shape and consists of igneous phases thought to be related to the evolution of the "1029" paleovolcano (Fig. 1). The composite igneous body is volumetrically dominated by four units, which have been recognised based on their texture and petrology of the least-altered drill-core samples studied. These are the rhyolitic and quartz porphyries, porphyritic monzogranite, and fine-grained monzogranite. The nature of the contact relationships of these units is not clear from the available diamond-drillhole core due to hydrothermal alteration (Fig. 4). Generally, however, the rhyolitic porphyry and fine-grained monzogranite are located in the upper part of the composite igneous body, where they form the most abundant rock types. The porphyritic monzogranite and quartz porphyry are present at depth and commonly below 600 m. Judging from the intense alteration and crosscutting mineralization, the rhyolitic porphyry is the earliest of the syn-mineralization intrusives. Post-mineralization stocks in the Chalukou composite igneous

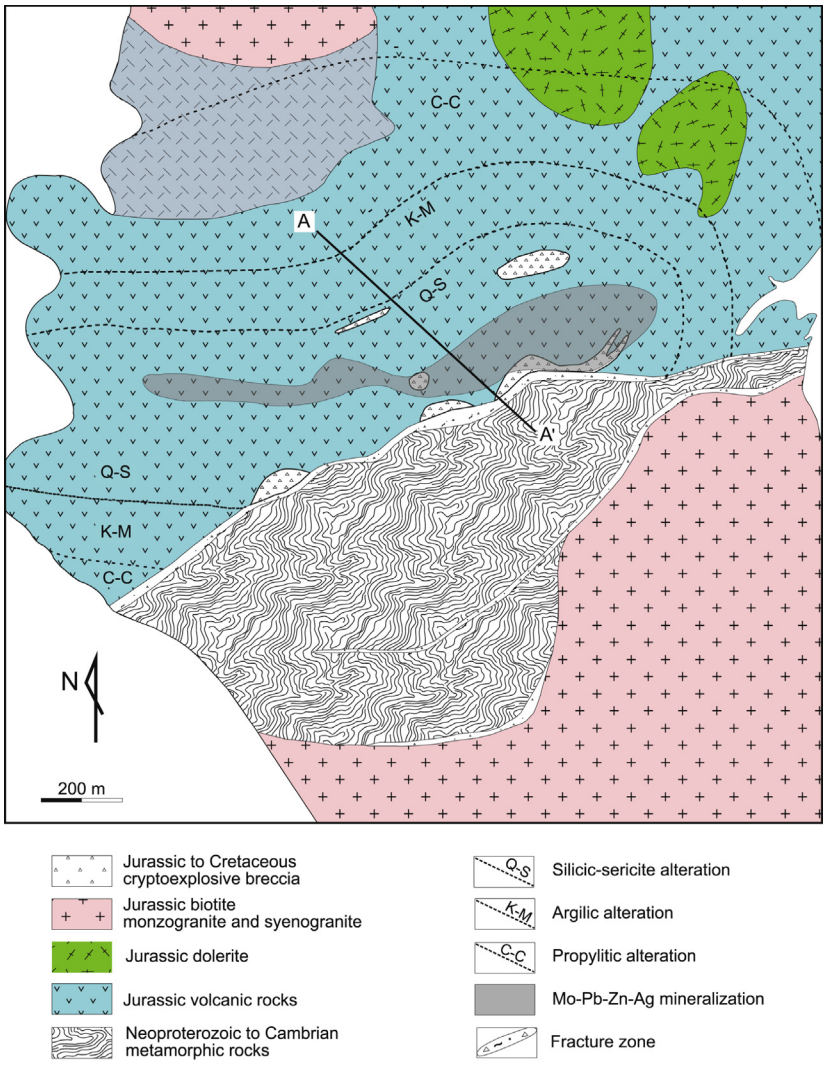

Fig. 2. Simplified geological map of the Chalukou deposit showing the main lithologies, faults, crypto-explosive breccia, hydrothermal alteration and Mo mineralization. Also shown is the location of Fig. 3 (modified after Liu et al., 2011).

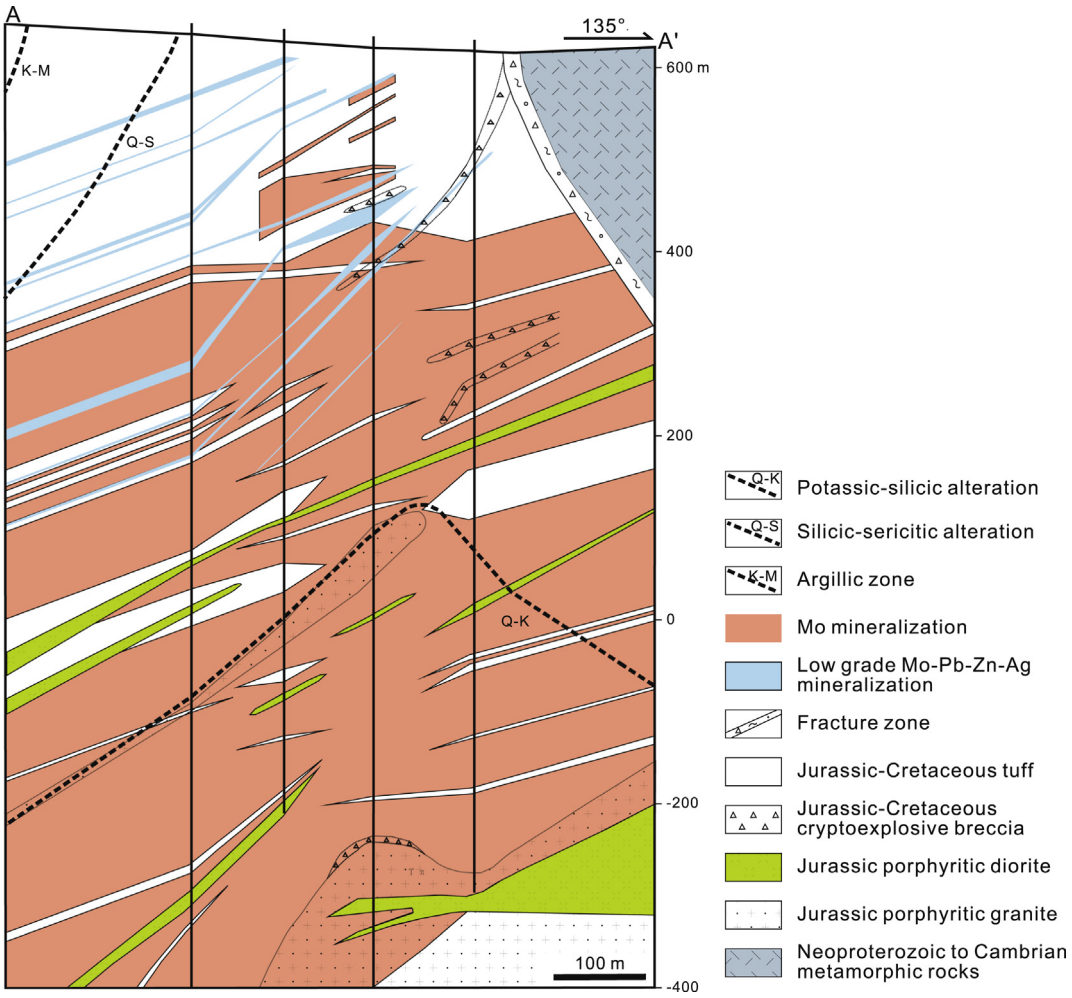

Fig. 3. Simplified cross-section A–A′ of the Chalukou deposit (modified after Liu et al., 2011).

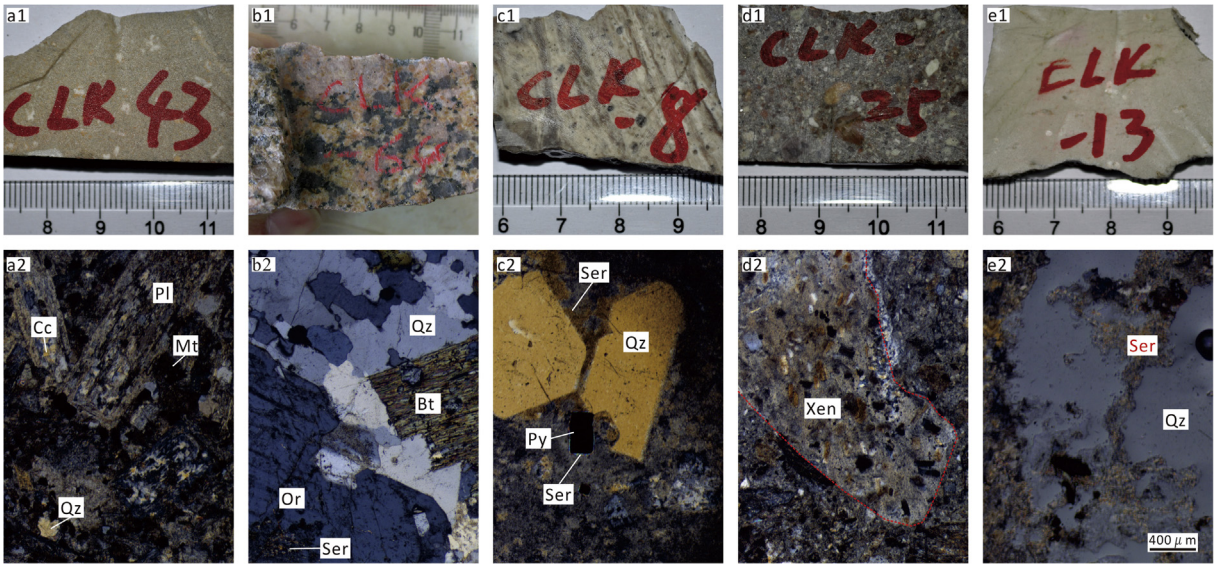

Fig. 4. Photographs of the main rock types at Chalukou and photomicrographs of rocks present in the mine area: (a1) hand specimen of carbonated dolerite; (a2) typical ophitic texture of diorite with most of the plagioclases (Pl) intensely altered to carbonate and pyroxenes altered to magnetite (Mt); (b1, b2) typical monzogranite present in the region; (c1) hand specimen of ore-forming-related rhyolitic porphyry; (c2) the matrix of the rhyolitic porphyry has undergone intense silicification and sericite alteration. The opaque mineral riming sericite is pyrite, showing that pyrite is a hydrothermal mineral; (d1) hand specimen of a volcanic rock representing post-mineralization magmatism; (d2) xenolith (Xen) of pre-mineralization diorite in a volcanic rock; (e1) quartz porphyry post-dating mineralization; and (e2) post-mineralization porphyry with intense hydrothermal alteration with corroded quartz (Qz).

body include the porphyritic monzogranite and syenogranite, and dioritic, andesitic and quartz porphyries. Hydrothermal alteration has destroyed primary igneous textures in these units, and feldspar phenocrysts are extensively altered to sericite, carbonate and quartz (Fig. 4).

Breccias are widely developed in the Chalukou region. The genesis of the breccias is attributed to the strong exsolution of fluids from cooling magma along hydrothermally controlled fractures. The breccia forms veins and pipes that are cemented by quartz or dark-coloured igneous material. The quartz-cemented breccia is paragenetically associated with the mineralization and the igneous breccia cemented by a relatively dark-coloured igneous matrix is closely associated with the post-mineralization intrusives.

3.2. Alteration

Hydrothermal alteration at Chalukou is temporally and spatially related to the emplacement of the Chalukou composite igneous body, and the alteration zone is present in an elliptical area that is >1800 m long and ~400–800 m wide. Alteration is zoned with a central K-silicate core that passes outward through phyllic and argillic to propylitic assemblages (Fig. 2).

The K-silicate alteration forms well-developed haloes at depths of >400 m (Fig. 3), which are composed of fine-grained quartz, K-feldspar, and variable proportions of biotite, magnetite and hematite. The hydrothermal alteration is commonly present along fractures as veins in the porphyritic monzogranite, and quartz and rhyolitic porphyries that are severely altered exhibiting grey, pink and red colours.

Widespread phyllic alteration characterized by the assemblage quartz–muscovite–fluorite(–pyrite) is peripheral to the K-silicate alteration and extends in an area that is 1200 m long, ~300–400 m wide, and ~800 m deep. This widespread alteration has destroyed the original textures of the intrusive and volcanic rocks, which are now pale grey-white, cream to pink coloured. Quartz veins with ~30 mm wide silica(–sericite) halos are a feature of the phyllic alteration in the deep parts of the deposit. The quartz veins commonly contain fluorite, molybdenite and pyrite at depth, but do not contain visible haloes of alteration assemblages in the upper part of the deposit.

The argillic alteration zone is characterized by the assemblage kaolinite–montmorillonite–chlorite–epidote–sericite–calcite, and is irregularly developed at the margin of the phyllic zone.

3.3. Mo-Pb-Zn-Ag mineralization

The mineralization is zoned vertically from a lower Mo-rich zone through a middle Pb-Zn-Ag zone with low-grade Mo, to an upper Pb-Zn-Ag-rich zone. The three zones also have distinctive ore styles with the lower Mo mineralization being a continuous and thick orebody, the middle Pb–Zn–Ag(–Mo) mineralization forming a stratiform orebody, and the upper Pb-Zn-Ag zone represented by ore veins.

Most of the Mo mineralization is present in the central parts of the deposit where intense K-silicate and phyllic alteration and a sulfide-bearing quartz stockwork are preferentially developed. The zone containing the Mo mineralization is >1800 m long, 200–1000 m wide, and extends from 180 to 980 m below the present-day surface (Fig. 3). The concentration of Mo increases gradually from the top of the deposit (with a cut-off grade of 0.03% Mo) towards the centre of the composite igneous body (with a relatively high-grade core of up to 0.15% Mo).

The Mo mineralization consists of thin molybdenite(–pyrite–fluorite–quartz) veins hosted by fractures or part of cement in breccia. The predominant sulfides are molybdenite and pyrite, minor amounts of sphalerite and galena, and trace amounts of chalcopyrite, magnetite and hematite. Molybdenite is present in thin quartz veins that are intergrown with pyrite as disseminated blebs and streaks. Typically, the veins have an inner quartz seam flanked by molybdenite and a diffuse phyllic halo. Larger aggregates of molybdenite are visible in quartz veins and along fractures, whereas, much of the molybdenite in the upper part of the composite igneous body forms in thin, discontinuous veins.

In general, the Zn-Pb-Ag mineralization is hosted by quartz veins dipping ~35°NW, forming a 1000–1700 m long zone that is up to 6 m thick, and extend vertically from a depth of 100 to 600 m. The veins are present in the upper part of composite body where they overlap the Mo mineralization as a relatively late-stage epithermal system. At least 27 veins containing Zn-Pb-Ag mineralization have been discovered and, although most are present above the Mo ore, some cross-cut low-grade Mo-bearing veins.

The Pb-Zn-Ag mineralization is relatively low grade, with the sulfide-bearing quartz veins having Zn–Pb combined grades of ~0.9–2.3%, and ~2.92–24.67 g/t Ag. Sulfide minerals in these veins include sphalerite, galena, molybdenite and pyrite, with minor amounts of pyrrhotite and chalcopyrite.

4. Sampling and analytical techniques

Five least-altered diamond-drillhole core samples, representing different igneous events in the Chalukou region, were sampled from dolerite (CLK43), biotite monzogranite (CLK64), rhyolitic porphyry (CLK8), tuff breccia from the Guanghua Formation (CLK25), and the post-mineralization quartz porphyry (CLK13) (Table 1). The samples were carefully selected for LA-ICP-MS U-Pb zircon geochronology to determine the relative ages of the samples.

The zircons analyzed were separated from 2 kg samples using traditional mineral separation techniques that included crushing, pulverizing, the use of a Wilfley Table, heavy liquid, magnetic separation, and handpicking. The samples were then mounted in epoxy and polished. Reflected and transmitted light photomicrographs, and cathodoluminescence (CL) images were used to determine the internal structures of sectioned zircon grains to target areas within the least-fractured and inclusion-free zones (Fig. 5).

U-Pb dating analyses were completed using a LA-ICP-MS at the Institute of Mineral Resources of the Chinese Academy of Geological Sciences in Beijing. Refer to Hou et al. (2009) for details on the operating conditions for the laser ablation system, the multi-collector inductively coupled plasma mass spectrometer (MC-ICP-MS) instrument. Laser ablation was performed using a Newwave UP 213 laser ablation system. A Thermo Finnigan Neptune MC-ICP-MS instrument was used to acquire ion-signal intensities. The array of four multi-ion-counters and three faraday cups allowed for simultaneous detection of ^{202}Hg(on IC5), ^{204}Hg, ^{204}Pb (on IC4), ^{206}Pb(on IC3), ^{207}Pb(on IC2), ^{208}Pb(on L4), ^{232}Th(on H2), and ^{238}U(on H4) ion signals. Helium was used as a carrier gas, and argon was used as the make-up gas that was mixed with the carrier gas via a T-connector before entering the instrument. Each analysis incorporated a background acquisition of approximately 20–30 s (gas blank) followed by 30 s data acquisition from the

Table 1
Location of samples collected for dating from the Chalukou deposit.

Sample	Rock type	Sample location
CLK-8	Rhyolitic porphyry	63.5 m of Drill hole ZKHD1803
CLK-13	Quartz porphyry	226 m of Drill hole ZKHD1803
CLK-25	Tuff breccia	528 m of Drill hole ZKHD901
CLK-43	Dolerite	455 m of Drill hole ZKHD1503
CLK-64	Monzogranite	51°09′33.3″N, 123°55′23.5″E

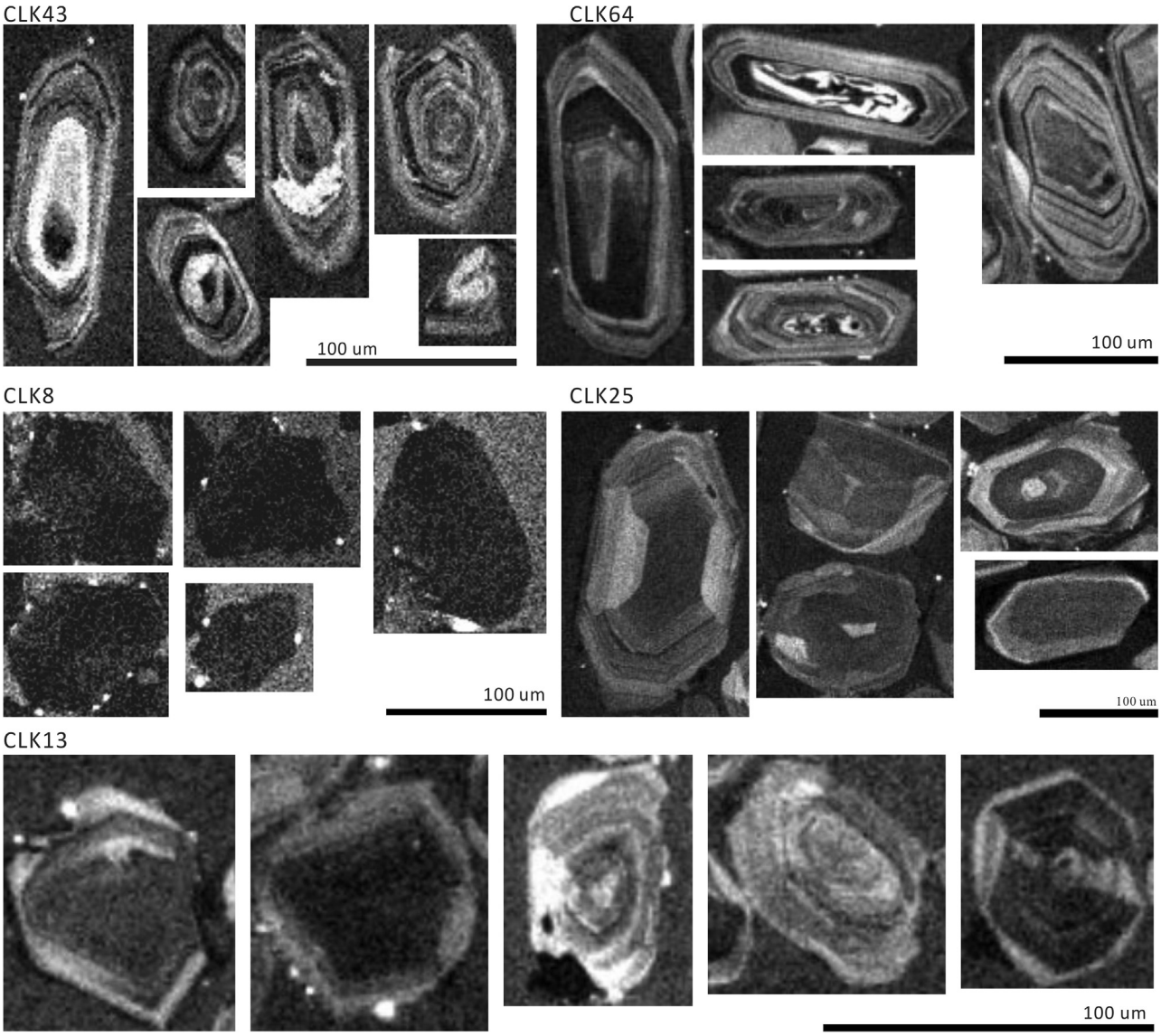

Fig. 5. Cathodoluminescence (CL) images of zircons dated from Chalukou.

sample. Off-line raw data selection, the integration of background and analyte signals, and time-drift correction and quantitative calibration for U-Pb dating were performed using *ICPMSDataCal* (Liu et al., 2010).

Standard zircon GJ1 was used as an external standard for U-Pb dating and was analyzed twice every 5–10 analyses. Time-dependent drifts of U-Th-Pb isotopic ratios were corrected using a linear interpolation (with time) for every 5–10 analyses according to the variations of GJ1 (i.e. 2 zircon GJ1 + 5–10 samples + 2 zircon GJ1; Liu et al., 2010). The preferred U-Th-Pb isotopic ratios used for GJ1 are from Jachon et al. (2004). The uncertainty of the preferred values for the external standard GJ1 was propagated to the ultimate results of the samples. In all analyzed zircon grains, the common Pb correction was not necessary due to the low signal of common ^{204}Pb and high ^{206}Pb/^{204}Pb values. The U, Th and Pb concentrations were calibrated using standard zircon M127 (with U: 923 ppm; Th: 439 ppm; Th/U: 0.475; Nasdala et al., 2008). Concordia diagrams and weighted mean calculations were made using Isoplot/Ex_ver3 (Ludwig, 2003). The Plesovice standard zircon was dated as unknown samples and yielded a weighted mean ^{206}Pb/^{238}U age of 337 ± 2 Ma (2σ, n = 12), which is in good agreement with the recommended ^{206}Pb/^{238}U age of 337.13 ± 0.37 Ma (2σ; Sláma et al., 2008).

5. Results

The zircon dates for the different samples from the Chalukou composite granite are presented in a series of concordia diagrams (Fig. 6; Table 2). The weighted mean ^{206}Pb/^{238}U dates were chosen as the age of the rocks, because the ^{207}Pb/^{235}U dates are biased by the uncertainty of the isotopic compositions of the corrected blank and common Pb content. Inherited zircons with older ^{206}Pb/^{238}U ages and zircons with a concordance of less than 90% were excluded from the age calculations (Table 2).

The dolerite sample (CLK43) has euhedral, colourless and transparent zircons that are 20–120 μm long, with length-width ratios of approximately 1:1 to 3:1. CL photographs reveal obvious fine concentric oscillatory zoning patterns and, rarely, sector zoning. Seven zircons were analyzed, and six analyses are sufficiently concordant to calculate the crystallization age for the dolerite. The ^{238}U and ^{232}Th concentrations are 135–191 ppm and 158–310 ppm, respectively, with Th/U ratios ranging from 1.13 to

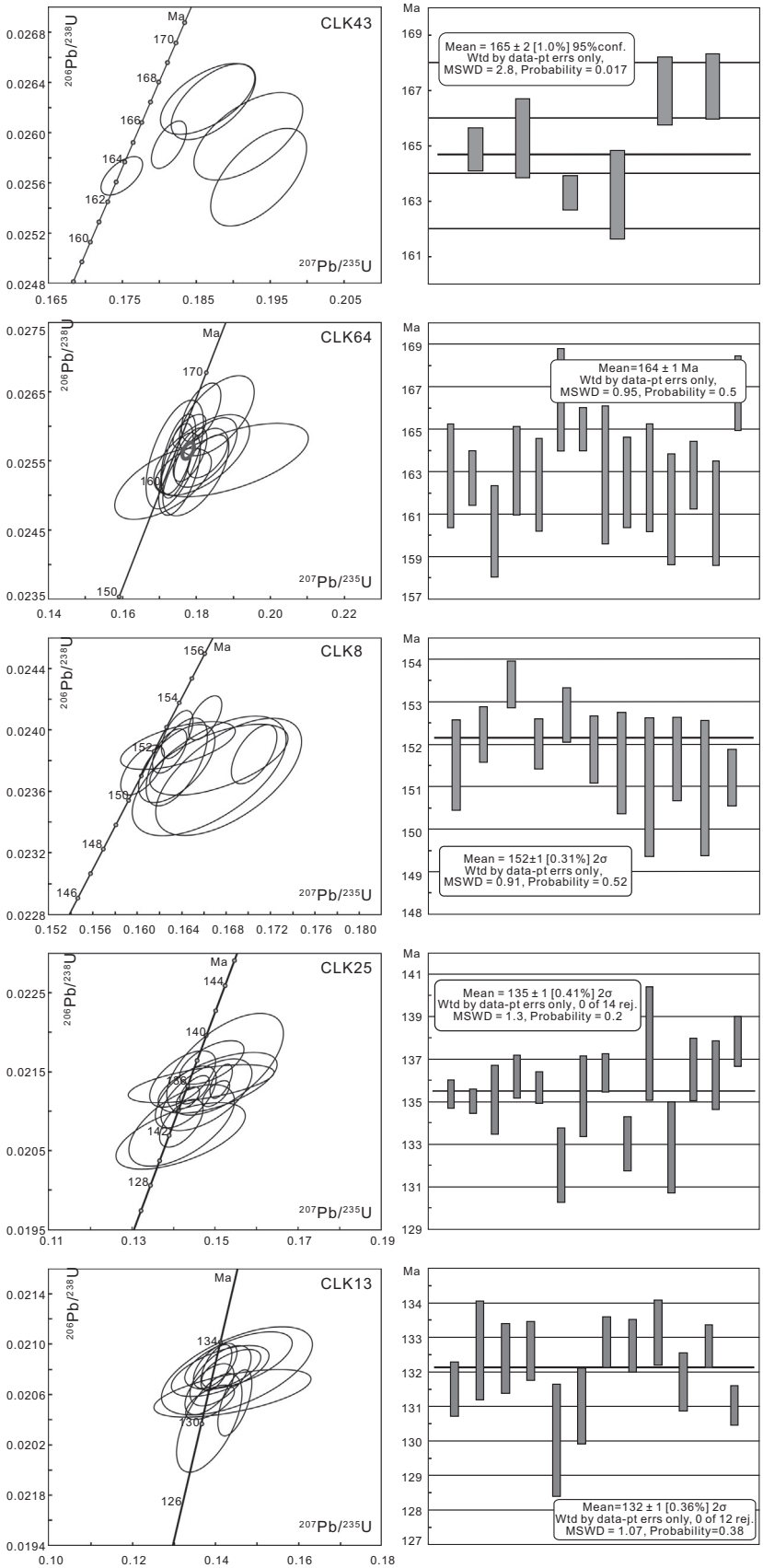

Fig. 6. Zircon U–Pb age plots for the Chalukou dolerite, granite, ore-forming rhyolitic porphyry and volcanic and post-mineralization porphyry.

Table 2
U–Pb zircon LA-MC-ICP-MS isotope data for magmatic rocks from the Chalukou deposit.

CLK43	Pb	^{232}Th	^{238}U	Th/U	^{207}Pb/^{206}Pb		^{207}Pb/^{235}U		^{206}Pb/^{238}U		^{208}Pb/^{232}Th		^{207}Pb/^{235}U		^{206}Pb/^{238}U		Concordance
	ppm	ppm	ppm	Ratio	Ratio	1σ	Ratio	1σ	Ratio	1σ	Ratio	1σ	Ma	1σ	Ma	1σ	
1	169.80	310.05	191.13	1.62	0.05079	0.00039	0.18137	0.00157	0.02591	0.00012	0.00161	0.00012	169.24	1.35	164.88	0.78	97%
2	118.26	315.31	135.07	2.33	0.05362	0.00128	0.19207	0.00487	0.02598	0.00023	0.00155	0.00020	178.39	4.15	165.31	1.43	92%
3	80.70	158.19	140.45	1.13	0.04943	0.00048	0.17495	0.00187	0.02566	0.00010	0.00255	0.00022	163.71	1.62	163.33	0.63	99%
4	161.30	306.33	166.25	1.84	0.05477	0.00116	0.19348	0.00429	0.02565	0.00025	0.00197	0.00023	179.60	3.65	163.25	1.60	90%
5	173.49	416.65	213.37	1.95	0.05173	0.00091	0.18728	0.00378	0.02625	0.00020	0.00152	0.00016	174.30	3.24	167.01	1.24	95%
6	54.95	71.48	67.48	1.06	0.05146	0.00109	0.18649	0.00425	0.02627	0.00019	0.00606	0.00091	173.63	3.64	167.19	1.17	96%
CLK64																	
1	28.50	101.32	95.29	1.06	0.05146	0.00235	0.18143	0.00850	0.02558	0.00039	0.00361	0.00044	169.29	7.30	162.84	2.43	96%
2	54.25	97.30	98.99	0.98	0.05196	0.00098	0.18307	0.00355	0.02557	0.00020	0.00313	0.00045	170.70	3.05	162.73	1.28	95%
3	5.62	17.38	21.05	0.83	0.04913	0.00231	0.17097	0.00859	0.02517	0.00034	0.01046	0.00194	160.26	7.44	160.23	2.15	99%
4	97.07	234.64	284.01	0.83	0.05177	0.00169	0.18263	0.00561	0.02562	0.00033	0.00193	0.00048	170.32	4.82	163.07	2.07	95%
5	21.24	61.47	66.88	0.92	0.05362	0.00088	0.30081	0.00564	0.04068	0.00032	0.00394	0.00071	267.03	4.40	257.05	1.99	96%
6	15.47	13.79	14.98	0.92	0.05440	0.00396	0.18968	0.01361	0.02551	0.00035	0.02210	0.00270	176.36	11.62	162.42	2.18	91%
7	40.28	57.37	50.06	1.15	0.05166	0.00214	0.18555	0.00675	0.02615	0.00038	0.00601	0.00163	172.83	5.78	166.42	2.39	96%
8	24.33	67.90	67.51	1.01	0.05222	0.00053	0.27561	0.00318	0.03829	0.00023	0.00397	0.00037	247.17	2.53	242.21	1.44	97%
9	11.89	50.66	59.27	0.85	0.04984	0.00078	0.17812	0.00293	0.02593	0.00016	0.00471	0.00048	166.44	2.52	165.02	1.02	99%
10	1.89	17.87	23.99	0.74	0.05262	0.00164	0.21080	0.00647	0.02923	0.00045	0.01572	0.00318	194.23	5.43	185.74	2.83	95%
11	0.45	22.96	27.90	0.82	0.05035	0.00148	0.17427	0.00508	0.02559	0.00052	0.01134	0.00219	163.12	4.40	162.89	3.25	99%
12	35.91	116.50	112.12	1.04	0.04974	0.00056	0.17484	0.00289	0.02553	0.00034	0.00263	0.00023	163.61	2.50	162.52	2.12	99%
13	46.61	160.14	118.63	1.35	0.04980	0.00049	0.17515	0.00305	0.02557	0.00040	0.00214	0.00018	163.88	2.64	162.75	2.53	99%
14	13.09	10.85	27.44	0.40	0.05162	0.00146	0.17992	0.00596	0.02533	0.00042	0.02590	0.00295	167.99	5.13	161.27	2.61	95%
15	38.87	90.49	99.21	0.91	0.05047	0.00061	0.17834	0.00296	0.02559	0.00025	0.00333	0.00031	166.63	2.55	162.87	1.60	97%
16	24.79	48.53	75.11	0.65	0.05034	0.00081	0.17548	0.00375	0.02531	0.00039	0.00597	0.00085	164.16	3.24	161.10	2.46	98%
17	95.75	271.56	236.77	1.15	0.05009	0.00061	0.18131	0.00354	0.02620	0.00028	0.00165	0.00014	169.19	3.05	166.73	1.75	98%
18	161.28	407.72	254.62	1.60	0.05212	0.00080	0.19517	0.00366	0.02715	0.00026	0.00169	0.00019	181.03	3.11	172.70	1.66	95%
CLK8																	
1	1196.01	835.35	496.52	1.68	0.04988	0.00059	0.16356	0.00225	0.02378	0.00017	0.00157	0.00012	153.81	1.97	151.52	1.06	98%
2	1269.93	984.24	637.47	1.54	0.04957	0.00087	0.16365	0.00340	0.02390	0.00010	0.00147	0.00007	153.89	2.96	152.25	0.65	98%
3	1923.20	1444.16	834.27	1.73	0.05004	0.00024	0.16610	0.00099	0.02408	0.00009	0.00158	0.00007	156.03	0.87	153.38	0.59	98%
4	1276.39	1021.46	738.76	1.38	0.04953	0.00025	0.16294	0.00103	0.02386	0.00009	0.00152	0.00007	153.27	0.90	152.02	0.59	99%
5	1389.04	1069.14	838.54	1.27	0.04952	0.00021	0.16362	0.00094	0.02397	0.00010	0.00162	0.00007	153.87	0.82	152.70	0.64	99%
6	995.95	897.12	632.95	1.42	0.05188	0.00033	0.17052	0.00137	0.02384	0.00012	0.00145	0.00009	159.87	1.19	151.89	0.79	94%
7	1696.04	1467.72	923.31	1.59	0.04990	0.00051	0.16360	0.00180	0.02379	0.00019	0.00156	0.00009	153.85	1.57	151.57	1.19	98%
8	796.14	854.68	516.91	1.65	0.05093	0.00099	0.16652	0.00454	0.02370	0.00026	0.00119	0.00009	156.40	3.96	151.00	1.63	96%
9	1707.68	1246.61	840.67	1.48	0.05096	0.00109	0.16737	0.00410	0.02381	0.00015	0.00157	0.00009	157.13	3.57	151.67	0.97	96%
10	1658.69	1205.78	757.63	1.59	0.05147	0.00107	0.16826	0.00432	0.02370	0.00025	0.00154	0.00012	157.91	3.75	150.98	1.60	95%
11	1452.76	1029.14	789.28	1.30	0.04904	0.00035	0.16050	0.00131	0.02374	0.00011	0.00152	0.00010	151.14	1.14	151.23	0.67	99%
CLK25																	
1	47.51	106.83	52.32	2.04	0.05148	0.00080	0.15018	0.00223	0.02122	0.00011	0.00284	0.00025	261.18	32.41	135.38	0.67	95%
2	43.01	173.33	90.20	1.92	0.04918	0.00063	0.14344	0.00187	0.02117	0.00009	0.00175	0.00015	166.75	29.63	135.05	0.57	99%
3	30.11	101.30	52.31	1.94	0.04897	0.00152	0.14304	0.00482	0.02118	0.00026	0.00301	0.00057	146.38	69.44	135.11	1.62	99%
4	21.80	83.41	45.76	1.82	0.04979	0.00376	0.14669	0.01157	0.02135	0.00016	0.00134	0.00046	183.42	170.35	136.20	1.01	97%
5	40.25	168.10	64.76	2.60	0.04957	0.00083	0.14511	0.00242	0.02127	0.00012	0.00190	0.00017	176.01	6.48	135.69	0.75	98%
6	3.50	77.85	48.95	1.59	0.04998	0.00399	0.14170	0.01024	0.02069	0.00028	0.00227	0.00049	194.53	174.05	132.04	1.76	98%
7	0.75	33.97	27.56	1.23	0.05080	0.00250	0.14792	0.00722	0.02121	0.00030	0.00561	0.00168	231.55	110.17	135.27	1. 90	96%
8	39.41	132.50	103.59	1.28	0.05144	0.00057	0.15149	0.00188	0.02138	0.00014	0.00215	0.00018	261.18	25.93	136.38	0.91	95%
9	29.43	83.76	40.75	2.06	0.04951	0.00121	0.14191	0.00356	0.02085	0.00020	0.00346	0.00041	172.31	52.77	133.04	1.27	98%
10	13.67	43.64	20.39	2.14	0.05187	0.00342	0.15245	0.00923	0.02160	0.00042	0.00638	0.00122	279.69	156.46	137.75	2.67	95%
11	30.20	46.02	30.39	1.51	0.04960	0.00281	0.14208	0.00841	0.02082	0.00034	0.00621	0.00129	176.01	131.46	132.86	2.14	98%
12	4.17	57.47	24.22	2.37	0.04834	0.00177	0.14216	0.00530	0.02141	0.00023	0.00467	0.00057	122.31	82.40	136.54	1.47	98%
13	19.61	26.75	14.56	1.84	0.05135	0.00318	0.15060	0.00940	0.02136	0.00026	0.00893	0.00105	257.47	144.43	136.26	1.62	95%
14	96.63	106.03	50.58	2.10	0.05011	0.00169	0.14925	0.00515	0.02162	0.00018	0.00398	0.00052	211.19	77.76500	137.86	1.16	97%
CLK13																	
1	93.61	153.99	55.10	2.79	0.04909	0.00328	0.14421	0.01246	0.02061	0.00012	0.00230	0.00019	136.79	11.06	131.51	0.79	96%
2	140.05	135.90	78.44	1.73	0.05062	0.00413	0.14522	0.01201	0.02079	0.00023	0.00236	0.00053	137.68	10.65	132.65	1.44	96%
3	91.25	293.39	83.41	3.52	0.04941	0.00175	0.14122	0.00487	0.02075	0.00016	0.00115	0.00020	134.13	4.33	132.41	1.00	98%
4	0.35	95.44	39.86	2.39	0.04868	0.00233	0.14108	0.00772	0.02079	0.00013	0.00287	0.00028	134.00	6.87	132.63	0.85	98%
5	64.02	90.15	54.17	1.66	0.04934	0.00185	0.13839	0.00519	0.02038	0.00026	0.00340	0.00067	131.61	4.63	130.03	1.63	98%
6	216.71	590.62	160.63	3.68	0.05112	0.00094	0.14469	0.00268	0.02053	0.00017	0.00102	0.00021	137.21	2.38	131.03	1.09	95%
7	333.56	851.90	214.73	3.97	0.04874	0.00119	0.13995	0.00349	0.02083	0.00012	0.00113	0.00009	133.00	3.11	132.89	0.73	99%
8	153.42	366.84	82.29	4.46	0.04896	0.00087	0.14028	0.00243	0.02081	0.00012	0.00124	0.00011	133.29	2.16	132.78	0.76	99%
9	0.84	318.95	93.86	3.40	0.05017	0.00246	0.14551	0.00851	0.02087	0.00015	0.00092	0.00014	137.94	7.54	133.16	0.93	96%
10	130.10	192.05	144.08	1.33	0.04870	0.00132	0.13861	0.00380	0.02064	0.00013	0.00238	0.00041	131.80	3.39	131.73	0.84	99%
11	103.13	162.49	83.69	1.94	0.04998	0.00149	0.14377	0.00471	0.02081	0.00010	0.00212	0.00021	136.39	4.18	132.76	0.62	97%
12	218.19	401.61	101.41	3.96	0.04880	0.00127	0.13858	0.00392	0.02054	0.00009	0.00124	0.00010	131.78	3.50	131.05	0.57	99%

2.33. The weighted mean ^{206}Pb/^{238}U age is 165 ± 2 Ma (with a MSWD of 2.8, Fig. 6), which corresponds to a Middle Jurassic crystallization age.

The porphyritic monzogranite sample (CLK64) has euhedral, colourless and clear zircons that are 50–200 μm long, and with length-width ratios of approximately 1:1 to 4:1. Small inclusions were observed in the transmitted light photomicrographs. There are obvious fine concentric oscillatory zoning patterns in most of the zircons, although some have obscure zoning patterns in their core indicative of inheritance. Eighteen zircons were analyzed,

with variable concentrations of ^{238}U (14–237 ppm), ^{232}Th (13–272 ppm), and Th/U ratios ranging from 0.83 to 1.60. Fourteen concordant analyses define a Middle Jurassic weighted mean $^{206}Pb/^{238}U$ age of 164 ± 1 Ma (with a MSWD of 0.95; Fig. 6). Four of the zircons have dates ranging from 257 to 172 Ma, which are interpreted as inherited zircons.

Rhyolitic porphyry sample CLK8 has euhedral, clear, colourless or light brown zircons that range from 20 to 150 μm in length, and have length to width ratios of approximately 1:1 to 2:1. Small inclusions were observed in the zircons on transmitted light photomicrographs and most are a deep, dark colour in CL photographs without concentric oscillatory zoning patterns. This interpreted to be due to enrichment in elements such as U and Th. Eleven analyses of transparent zircon grains were analyzed from which 11 concordant analyses formed a cluster on the relative probability plot with a weighted mean $^{206}Pb/^{238}U$ age of 152 ± 1 Ma (MSWD = 0.91; Fig. 6). These data have variably high contents of ^{232}Th (835–1468 ppm) and ^{238}U (496–923 ppm), with Th/U ratios between 1.27 and 1.73.

Zircons from sample CLK25 of a volcanic rock from the Guanghua Formation are commonly clear, colourless, euhedral, and 80–250 μm long with length to width ratios of 1:1 to 2:1. Small inclusions were observed in the zircons on the transmitted light photographs, and most have fine concentric oscillatory zoning patterns on CL photographs, and inherited zircons in cores of the zircons have a wide oscillatory zonation. Nineteen analyses of the transparent zircons indicate that they have relatively low contents of ^{232}Th (33–173 ppm) and ^{238}U (20–90 ppm) with Th/U ratios ranging from 1.23 to 2.60. Fourteen of the analyses are concordant with a weighted mean $^{206}Pb/^{238}U$ age of 136 ± 1 Ma (MSWD = 1.3, Fig. 6). Five inherited zircons have older ages ranging from 161 to 138 Ma.

Quartz porphyry sample CLK13 has clear, colourless and euhedral zircons that are ~20–100 μm long, and have length-to-width ratios of approximately 1:1 to 2:1. CL images of the zircons reveal fine concentric oscillatory zoning patterns and rare sector zoning. Twelve analyses of transparent zircons have low abundances of ^{232}Th (21–152 ppm) and ^{238}U (20–82 ppm), and Th/U ratios between 1.04 and 2.19, have a weighted mean $^{206}Pb/^{238}U$ age of 132 ± 1 Ma (MSWD = 1.07, Fig. 6). This dating indicates that the quartz porphyry was emplaced during the Early Cretaceous and provides a younger limit to the timing of the Mo mineralization.

6. Discussion

6.1. Deposit classification

Porphyry Mo deposits are subdivided into two types based on the chemistry of their associated pluton and tectonic setting (Mutschler et al., 1981; Westra and Keith, 1981; White et al., 1981; Carten et al., 1993; Audetat, 2010). The first type includes low-grade low-F porphyry Mo deposits that are hosted by granodiorite, arc-related and associated with calc-alkaline magma. The second type includes high-grade high-F porphyry Mo deposits hosted by extension-related monzogranite, and associated with highly evolved rhyolitic magma (Ludington and Plumlee, 2009, Ludington et al., 2009; Pirajno and Zhou, 2015).

Based on the geology of the Chalukou deposit and studies from the literature, we suggest that the deposit is a high-F-type porphyry Mo deposit, because:

(1) The Chalukou deposit commonly contains fluorite in its upper section part, which indicate there is a relatively high-F fugacity in the initial Chalukou ore fluid, and <100 ppm F has been analyzed in fluid inclusions from the deposit (Xiong et al., 2014). In addition, there are numerous Mesozoic fluorite deposits in the XMO, such as the Sumu Tsagaan Obo, Hailimin and Dongfanghong fluorite deposits (Xu et al., 2008).

(2) Rare metals concentrated in the ore system (e.g. Sn and W) characterize the Climax-type high-F Mo deposits in Colorado, and some of the deposits have associated Ag-rich polymetallic veins (Ludington and Plumlee, 2009). There is significant Zn-Pb-Ag mineralization in the shallow part of the Chalukou deposit (Fig. 3), which is a characteristic similarity to Climax-type high-F Mo deposits. Although the Chalukou deposit doesn't contain significant Sn and W, it is noteworthy to mention here that Sn-W mineralization is well-developed in the XMO, such as the Weilasituo porphyry Sn-W-Rb, Huanggangliang Sn-Fe skarn, and Shamai W, and Honghuaerji greisen W deposits (Nie et al., 2011; Zhou et al., 2012; Xiang et al., 2014; Liu et al., 2016), which indicate the region is also rich in rare metals.

(3) The Chalukou deposit is genetic related to highly fractionated and an evolved magma source. Fractional crystallization plays a key role in forming highly evolved felsic magmas and leads to a high Mo content in high-F-type Mo deposits (Audetat, 2010). Geochemical studies show that granites at the Chalukou deposit are highly fractionated and I-types with a degree of fractionation that is similar to Climax-type granites (Westra and Keith, 1981; Li et al., 2014; Liu et al., 2015).

(4) Geochemical studies indicate that the Chalukou was formed in intra-plate extensional or post-collision extensional tectonic settings (Li et al., 2014; Liu et al., 2015). In addition, the presence of Jurassic to Cretaceous highly evolved I-type granites, Late Triassic to early Cretaceous A- type granites and Mesozoic bimodal volcanic rocks in the North Great Xing'an Range also indicate that the Chalukou deposit formed in an extensional setting (Jahn et al., 2001; Wu et al., 2002; Lin et al., 2003; Wu et al., 2003a,b). Although an extension tectonic setting is favoured for the deposition of high-F-type Mo deposits, because the setting associated with highly evolved source magma, the Mesozoic extension in the study region was probably triggered by a post-orogenic extension or tectono-thermal event during the Mesozoic and after subduction of the Paleo-Asian Oceanic Plate beneath the NCC during the Paleozoic (Jahn et al., 2001; Meng, 2003; Pirajno and Zhou, 2015), rather than a rift setting, as is the case in the Oslo continental rift of Norway, the volcanic-rifted margin of east Greenland and Rio Grande rift in Colorado (Schönwandt and Petersen, 1983; Brooks et al., 2004; Ludington and Plumlee, 2009; Audetat, 2010; Chapin, 2012). The difference between these settings may be the reason why porphyry Mo deposits in Colorado have a higher Mo grade than the porphyry Mo deposits in North Great Xing'an Range.

6.2. Concentrations of U and Th in zircons as indicators for the evolution of Mo concentration in the source magma for the Chalukou deposit

The concentrations of Mo in siliceous melts of a rhyolitic composition are low and the enrichment of Mo in these melts is possibly achieved through fractional crystallization and the interaction and movement of magmatic-hydrothermal fluids (Audetat, 2010; Audetat et al., 2011). The Chalukou deposit is part of a multiphase magmatic intrusion that is has been gone through strong fractional crystallization over a relatively long period in time forming the composite granite (Li et al., 2014; Liu et al., 2015). Although intense alteration at Chalukou, especially at depth, has masked the primary

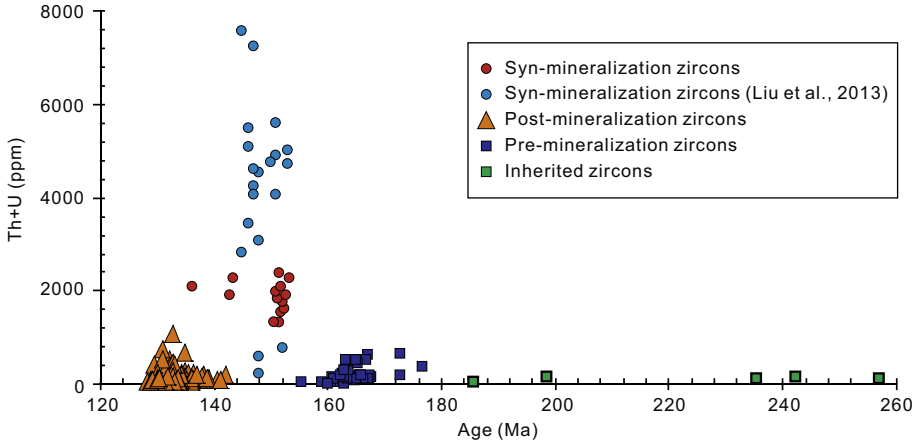

Fig. 7. A plot of Th + U (ppm) vs ages (Ma) showing the high Th + U concentration of zircons from the ore-forming rhyolitic porphyry compared to zircons from pre- and post-mineralization.

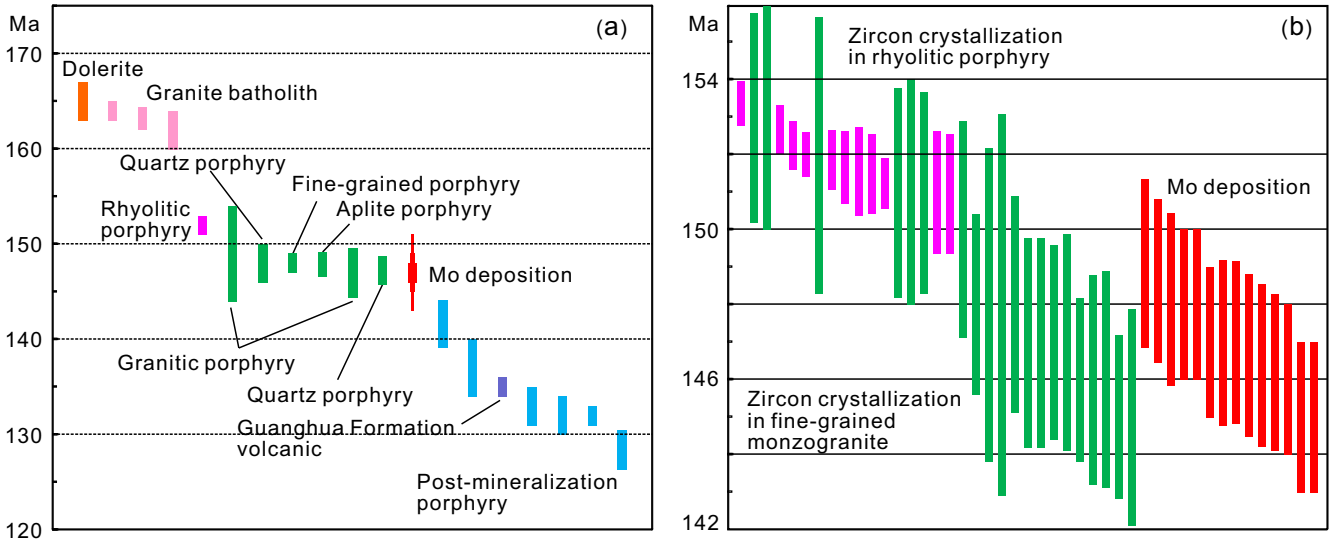

Fig. 8. A summary of: (a) major geological events at Chalukou (Nie et al., 2011; Liu et al., 2014 and this study); and (b) the zircon crystallization ages of the ore-forming magma and deposition ages of molybdenite (Nie et al., 2011; Liu et al., 2014; this study).

igneous mineralogy of the granites, the rhyolitic porphyry (sample CLK8) has been recognized as being the earliest magmatic phase associated with Mo mineralization. This is evident from the presence of pyrite and Mo in the upper part of the composite granite. U-Pb zircon dating of this rock indicates that the Th and U concentrations in zircons are 4.5–18.9 (averaging ~15) times higher than for zircons from samples of the pre- and post-mineralization intrusives (Table 2; Fig. 7). It is noted that zircons from the mineralization-related porphyritic monzogranite also have relatively very high concentrations of U and Th with a combined average of 3093 ppm or 0.31% (Fig. 7; Liu et al., 2013, 2014). Given that the high-field-strength elements Mo, Th, U, and Zr have a similar chemical behaviour principally due to non-bridging oxygen within the silicate melt structure (Lowenstern et al., 1993), the concentration of Th and U in zircons is a useful marker for the enrichment of Mo concentration in the magma. This indicates that the porphyry rocks containing zircons with elevated Th and U concentrations are directly associated with ore-fluid exsolution. In the case of the Chalukou deposit, the elevated Th and U concentration in zircons from sample CLK 8 indicates a genetic association between the melt (represented by the rhyolitic porphyry) and porphyry Mo-Pb-Zn-Ag mineralization.

6.3. A protracted porphyry Mo mineralization system in a long-lived magmatic evolution cycle

Eleven analyses of zircons for the rhyolitic porphyry Sample CLK8 yield ages ranging from ca. 153 to 151 Ma and have a weighted mean $^{206}Pb/^{238}U$ date of 152 ± 1 Ma, which is interpreted as the crystallization age of the porphyry (Table 2, Fig. 8b). Given that the emplacement of the rhyolitic porphyry represents the early stage of the Chalukou mineralization, the magmatism related to the mineralization began at ca. 152 Ma.

Recent high-resolution Re-Os geochronology on molybdenite samples separated from quartz-molybdenite veins at Chalukou yield isochron ages of 147 ± 1 and 148 ± 1 Ma (Table 3, Nie et al., 2011; Liu et al., 2014). We recalculated these combined Re-Os data giving a molybdenite isochron age of 147 ± 1 Ma (Fig. 9; Table 3). Although the Re-Os isochron age represents the average deposition age of molybdenite from Chalukou, it is suggested that the molybdenite model age has a higher internal precision (<0.2%) than the molybdenite Re-Os isochron age (<0.6%) (Chiaradia et al., 2013). The Re-Os isochron age of 147 ± 1 Ma, therefore, probably represents an average deposition age for molybdenite at the Chalukou deposit. The combined Re-Os model ages have a wide range

Table 3
Re-Os data of molybdenite from the Chalukou deposit.

Sample	Re (ppm)		187Re (ppb)		187Os (ppb)		Model age		Reference
	Measured	2σ	Measured	2σ	Measured	2σ	Measured	2σ	
CLK-16	36.44	0.33	22.91	0.21	56.16	0.5	147	2	Nie et al., 2011
CLK-20	11.79	0.11	7.41	0.07	18.38	0.15	149	2	
CLK-28	4.52	0.04	2.84	0.03	7.062	0.063	149	2	
CLK-30	88.48	0.83	55.61	0.52	136.3	1.1	147	2	
CLK-31	8.22	0.07	5.17	0.04	12.65	0.12	147	2	
CLK-33	33.76	0.29	21.22	0.18	51.81	0.48	146	2	
CLK-61	1.7	0.02	1.07	0.01	2.638	0.024	148	2	
CLK-63	44.68	0.39	28.08	0.24	68.48	0.54	146	2	
HD-7	2.5	0.0	1.6	0.0	3.8	0	145	2	Liu et al., 2014
HD-9	4.0	0.0	2.5	0.0	6.1	0.1	145	2	
HD-213	23.5	0.2	14.8	0.1	35.9	0.1	146	2	
HD-54	20.2	0.2	12.7	0.1	31.4	0.3	148	2	
HD-252	21.7	0.2	13.6	0.1	33.5	0.3	147	2	
HD-55	9.6	0.1	6.0	0.0	14.8	0.1	148	2	

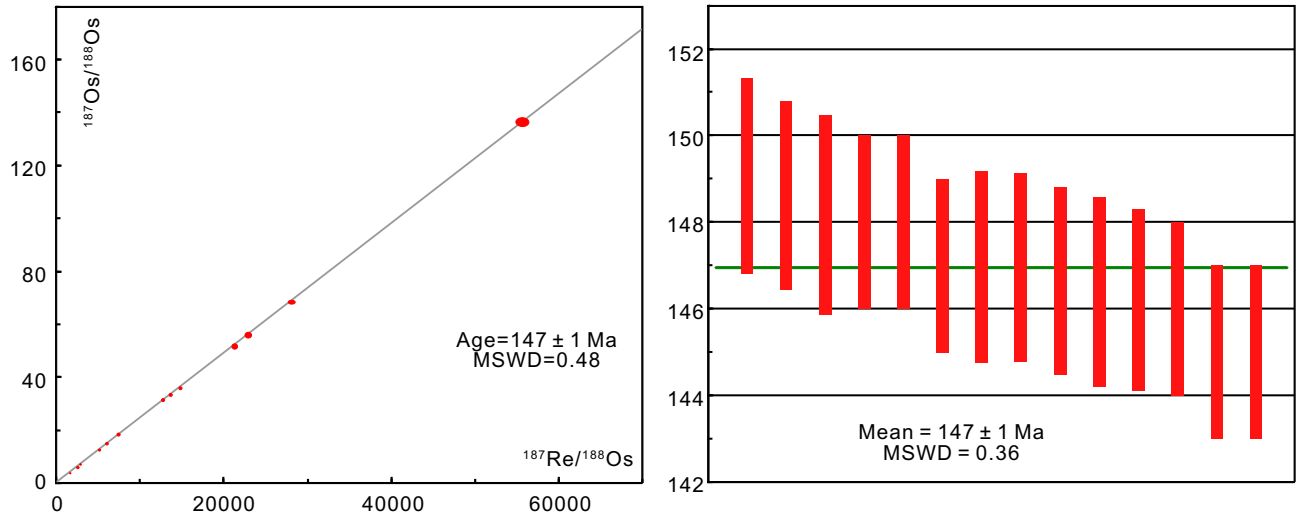

Fig. 9. Re-calculated Re-Os isochron age and weighted mean model age based on the studies of Nie et al. (2011) and Liu et al. (2014).

Table 4
Summary of ages in thChalukou porphyry Mo deposit.

Rocks	Occurrence	Age	Method	References
Dolerite	Dyke	165 ± 2	Zircon La-ICP-MS dating	This study
Monzogranite	Batholith	172.4 ± 1.6	Zircon La-ICP-MS dating	Li et al., 2014
Monzogranite	Batholith	164 ± 1	Zircon La-ICP-MS dating	This study
Monzogranite	Batholith	163.2 ± 1.2	Zircon La-ICP-MS dating	Li et al., 2014
Monzogranite	Batholith	162 ± 2	Zircon La-ICP-MS dating	Liu et al., 2014
Rhyolitic porphyry	Sub-volcanic	152 ± 1	Zircon La-ICP-MS dating	This study
Granitic porphyry	Stock	149 ± 5	Zircon La-ICP-MS dating	Liu et al., 2014
Quartz porphyry	Stock	148 ± 2	Zircon La-ICP-MS dating	Liu et al., 2014
Fine- grained granite	Stock	148 ± 1	Zircon La-ICP-MS dating	Liu et al., 2014
Aplite porphyry	Stock	147.9 ± 1.3	Zircon La-ICP-MS dating	Li et al., 2014
Granitic porphyry	Stock	147 ± 2.6	Zircon La-ICP-MS dating	Li et al., 2014
Quartz porphyry	Stock	147.3 ± 1.5	Zircon La-ICP-MS dating	Li et al., 2014
Molybdenite	Quartz vein	147 ± 1	Re-Os isochron dating	Re-calculated based on Nie et al., 2011; Liu et al., 2014
Dioritic porphyry	Stock	141.7 ± 2.5	Zircon La-ICP-MS dating	Li et al., 2014
Rhyolitic porphyry	Sub-volcanic	137 ± 3	Zircon La-ICP-MS dating	Liu et al., 2014
Tuff breccia	Volcanic	135 ± 1	Zircon La-ICP-MS dating	This study
Dioritic porphyry	Stock	133 ± 2	Zircon La-ICP-MS dating	Liu et al., 2014
Andesitic porphyry	Stock	132 ± 2	Zircon La-ICP-MS dating	Liu et al., 2014
Quartz porphyry	Stock	132 ± 1	Zircon La-ICP-MS dating	This study
Quartz monzogranite porphyry	Stock	128.4 ± 2.1	Zircon La-ICP-MS dating	Li et al., 2014

between 149 ± 2 and 145 ± 2 Ma, and indicate that the molybdenite at Chalukou might have a protracted deposition history lasting around 5 million years, and combined with the intrusion age of the rhyolitic porphyry, this also indicates that there is a protracted ore-related magmatic-hydrothermal history lasting around 7 Ma (Table 3, Nie et al., 2011; Liu et al., 2015).

The U-Pb zircon geochronological data presented above for the Chalukou composite igneous body broadly reflect a long lived magmatism starting at ca. 165 Ma and continuing to ca. 145 Ma during the latest stage of Mo mineralization and then during another magmatic cycle to ca. 136 Ma after the Mo mineralization terminated. In detail, the magmatism can be divided into an early progressive event and a later waning event. The early event is represented by the ca. 165 Ma dolerite and ca. 162 Ma monzogranite and syenogranite, which waned with the intrusion of ca. 152 Ma rhyolitic porphyry, porphyritic monzogranite, quartz porphyry, fine-grained monzogranite and deposition of molybdenite and base metals by ca. 145 Ma. This was followed by the emplacement of the post-ore quartz porphyry and another volcanism cycle represented by the Guanghua Formation (Fig. 8a; Table 4).

7. A proposed model

7.1. Metal introduction during protracted and progressive magmatism

In many porphyry Mo deposits, mineralization is directly associated with small volumes of porphyry emplaced as stocks (e.g. Chalukou Mo deposit; Nie et al., 2011; Liu et al., 2011; Henderson Mo deposit, Carten et al., 1988). However, numerous authors have suggested that a volume of more than 20 to 100 km^3 of melt is required to concentrate large amounts of metals to produce an economic porphyry deposit such as the Chalukou Mo deposit (Keith et al., 1986; Cline and Bodnar, 1991; Lowenstern, 1994; Shinohara et al., 1995; Klemm et al., 2008; Audetat, 2010; Lerchbaumer and Audétat, 2013). The minimum volume of a fluid-generating magma needed to form such a major deposit is tens to hundreds of km^3 (Quadt, 2011).

Many porphyry Mo mineralization belts around the world have undergone the same long-period and multiphase igneous activity. For example, the porphyry Mo deposits in the Colorado molybdenum mineral belt of the USA, the east Greenland rifted continental margin, and the Oslo rift are associated with evolved and highly fractionated granites that formed after the peak activity of a magmatic cycle (Chapin, 2012; Ludington and Plumlee, 2009; Brooks et al., 2004; Carten et al., 1988; Schönwandt and Petersen, 1983; Wallace et al., 1978). In addition, numerous giant high-F-type porphyry deposits, such as the Henderson porphyry Mo deposit in Colorado, also have undergone multiphase magmatic events when they were being formed (Carten et al., 1988).

It is suggested that magnetite, ilmenite, titanite, pyrrhotite and biotite are enriched in and are the largest reservoirs of Mo in crustal rocks (Bingen and Stein, 2003; Audetat, 2010; Audetat et al., 2011). Consequently, the breakdown of these minerals during partial melting can liberate a significant amount of Mo (Bingen and Stein, 2003). Multiphase partial melting and melt extraction from the lithospheric mantle may be an effective mechanism for the formation an ore-forming large magma chamber in the lower crust (Pettke et al., 2010). Heat flow levels, however, are lower in post-orogenic tectonic settings than in subduction settings, so it will take relatively longer to form a large enough magma chamber at upper crustal levels. A long-lived and multistage magmatic evolution is also needed to concentrate the metals to economic grades. In this process, multistage and long-lived magmatic differentiation in different crust levels may help to generate the evolved magma observed in most of porphyry Mo deposits worldwide, and the gradual collection of incompatible ore-forming metals, such as Mo in magma chambers in the upper crust (Lowenstern et al., 1993; Audetat et al., 2011). In this scenario, compatible elements such as Cu form a residue in the solid phase during the extraction of more differentiated proportions of a magma (e.g. Candela and Holland, 1986). This might be one of the reasons why high-F-type porphyry Mo deposits hosted by highly differentiated granitic rocks have high Mo/Cu ratios.

The passage of large amounts of metals from huge volumes of magma to shallow depths, where deposits are located, necessitates a transportation mechanism, such as a convective fluid-flux in a fluid- or gas-rich magma (Keith et al., 1986; Candela and Holland, 1986; Lowenstern et al., 1993; Lowenstern, 1994). It is suggested that slow crystallization rates and a long-lived convection in silicic magma are required to transport Mo-bearing volatile components from large magma chambers to shallow sites of deposition (Shinohara et al., 1995).

In the case of the Chalukou example, the whole-rock and isotopic geochemistry of the magmatic units indicate that they are highly fractionated, and have very similar Hf-Sr-Pb isotope characteristics (Li et al., 2014; Liu et al., 2015), which suggest that these

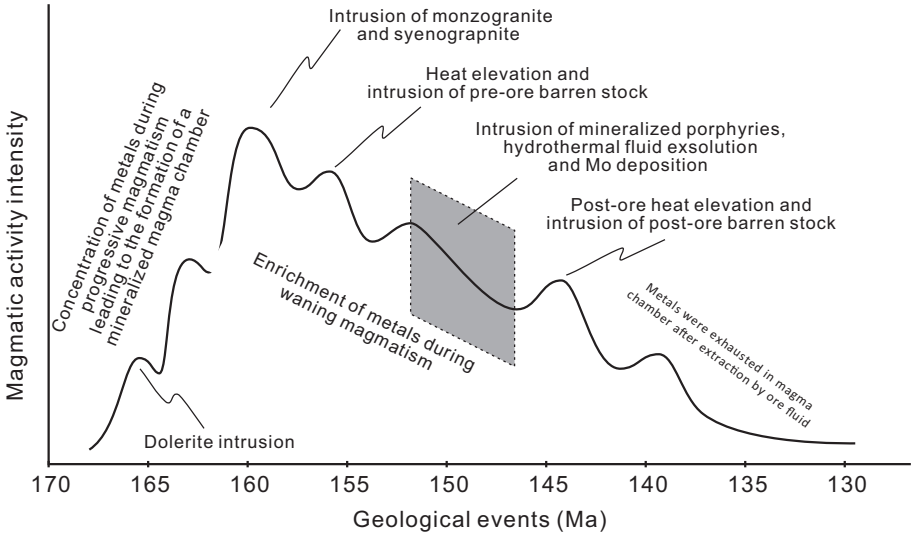

Fig. 10. Simplified model showing the magmatic-hydrothermal evolution and mineralization in the Chalukou region. The geological events at Chalukou are divided into a progressive and waning magmatism. The progressive phase involved the introduction of metals and the waning phase represents enrichment of the metals. The chart shows that the formation of the giant porphyry Mo deposit at Chalukou is not an isolated geological event related to small volume porphyry stocks, but is a long-lived magmatic event.

rocks are derived from the same magma chamber. The progressive, intensive and long-lived evolution of magmatic processes from ca. 165 to 147 Ma before fluid exsolution, are indicative of a deep and large-scare magma chamber beneath the Chalukou porphyry Mo deposit. It is suggested that the size of magma chamber is a key factor forming an economic porphyry Mo deposit, because of the low saturation concentration of Mo in granitic melt (Lerchbaumer and Audétat, 2013). Hence, the progressive magmatism discussed above is envisaged to reflect a history of the progressive introduction of metals from deep levels to form a Mo-rich magma chamber, and further support a long-lived magmatism in the Chalukou district.

7.2. Metal enrichment during protracted and waning magmatism

Studies on the composition of melt inclusions show that fractional crystallization is the important mechanism for the formation of an evolved magma and the concentration of Mo in a melt (Audetat, 2010; Audetat et al., 2011). Magmatism in the Chalukou region underwent waning between the solidification of the ca. 164 Ma biotite monzogranite to the emplacement of the ca. 152 Ma rhyolitic porphyry, and the exsolution of Mo-bearing fluids by ca. 145 Ma. This reflects a sustained and gradually weakened input of magma and heat from a deep-seated magma chamber. The concentration of U and Th in zircons also shows an increase from an average value of 207 ppm (or 0.02%) for pre-mineralization porphyry rocks to an average value of 3093 ppm (or 0.31%) for the syn-mineralization rhyolitic porphyry (Fig. 7), which equates to a ~15 time enrichment in the concentration of U and Th in the syn-mineralization rhyolitic porphyry compared to the pre-mineralization porphyry, and is indicative of an intensive enrichment of metals in the magma chamber. Hence, the waning magmatism at Chalukou is here considered crucial for the formation of a protracted porphyry Mo ore-forming event at Chalukou for the following reasons:

(1) The waning magmatism could have resulted in fractional crystallization in the proposed large magma chamber beneath the porphyry Mo deposit. A slow and long fractional crystallization will result in the concentration of HFSEs, LILEs and volatiles, finally leading to the formation of highly evolved and volatile-rich magma associated with porphyry Mo mineralization (during the late stage of magmatism).
(2) The sustained, although gradually weakened, input of magma and heat will provide a kinetic regime that maintains fractional crystallization and the convection of the highly evolved magma associated with porphyry Mo mineralization in a long-time span.
(3) A long-lived Rayleigh fractionation of volatiles from the ore-forming magma will lead to the saturation and exsolution of fluid during the late stage of magmatism, and Mo will be concentrated in fluid phases due to its fluid or melt partition coefficients ($D_{Mo,\ fluid/melt}$ = 17–20; Audetat, 2010).
(4) The sustained convection of ore-forming magma is favourable for the transportation of metal-rich fluid with magma to the uppermost parts of the magma chamber, and the release of this metal-rich fluid would lead to hydrothermal alteration and metal deposition (Shinohara et al., 1995).
(5) The concentration of fluid will also lead to the build-up of overpressure in the ore-forming system, which may cause the explosion and formation of hydrothermal breccia.
(6) The magma chamber is becomes depleted after metals have been extracted to the mineralization sites at shallow parts of the ore system by the exsolved metallic fluid, which eventually end with the post-ore porphyries being barren.

These interpretations are supported by the presence of the multiphase porphyry intrusions and the protracted period of around 7 million years for the Mo mineralizing event at Chalukou. The elevated U and Th concentration in the zircons from the rhyolite porphyry and fine-grained monzogranite indicates enrichment in HFSEs in the evolving magma (Fig. 7), which may be due to the long-lived differentiation of the magma chamber. The sustained and episodic input of magma and heat would also have caused thermal disturbance and the emplacement of multiphase porphyry intrusions, triggered the partial remelting of consolidated magma, and repeatedly extraction of metals from residual or fractionated melts in the magma chamber.

We propose a scenario in which the large quantities of metals needed to form a giant porphyry Mo polymetallic deposit at Chalukou is enriched in a long-lived magmatic evolution that progressed from progressive to waning phases. A protracted ore-forming history is favoured for the formation of giant porphyry Mo deposits, which may also be why a large volume of melt is required for the formation of such giant porphyry Mo deposits, even they may appear to be genetic related to small igneous stocks that are probably like 'tips to the iceberg'. The genesis scenario of Chalukou porphyry Mo-(Pb-Zn-Ag) deposit is graphically summarized in Fig. 10.

8. Conclusions

The Chalukou is a high-F-type porphyry deposit hosted by and genetically associated with the multiphase Chalukou composite igneous body. Detailed LA-ICP-MS U-Pb zircon geochronology indicates that the ore-related porphyry rhyolite was emplaced at 152 ± 1 Ma. Coupled with published molybdenite Re-Os ages of ca. 149 to 145 Ma (Nie et al., 2011; Liu et al., 2014), these new data suggest that Chalukou is a protracted porphyry ore-forming system lasting some 7 Ma. The elevated U and Th concentrations in zircons show a gradually increase from 27 to 662 ppm (average at 207 ppm) for pre-mineralization porphyry rocks to 228–7582 ppm (average at 3093 ppm) for syn-mineralization rhyolitic porphyry rocks, and then decrease to 33–1067 ppm (average at 183 ppm) for post-mineralization porphyry rocks. The concentration of Th and U in zircons is therefore a useful indicator of the Mo concentration and evolution in the magma, and indicates that porphyry rocks with zircons containing high Th and U concentrations are directly associated with ore fluid exsolution.

New zircon data presented here suggest that there is a long-lived magmatism in the Chalukou region with the earliest magmatism resulted in the emplacement of small mafic intrusions of dolerite stocks at ca. 165 Ma. This was followed by the emplacement of an extensive monzogranitic and syenogranitic intrusion at ca. 164 Ma, and was followed by waning magmatism with the emplacement of a syn-mineralization rhyolitic porphyry at ca. 152 Ma. The mineralized magmatism was succeeded by barren Early Cretaceous magmatism that formed extensive volcanic sequences including the Guanghua Formation at ca. 136 Ma. Most of the porphyries that were emplaced during the post-mineralization stage of magmatism have ages younger than ca. 152 Ma.

Multiphase igneous activity in a long-lived magmatism may play a crucial role in the formation of a large-volume magma chamber are necessary for the eventual concentration of metals forming the giant Chalukou porphyry Mo deposit. In addition, the protracted and waning stage of the magmatic evolution in the area is here considered vital for the transportation and enrichment of metals at Chalukou.

Acknowledgements

This study was financially supported by funds from the Chinese State 973 Project (2013CB429805), and Chinese NSFC Project (41302057). We are grateful to Dr Sean J. O'Brien, Dr Peter C. Lightfoot, Dr Liu and Dr Sun for their constructive suggestion that significantly improved the manuscript.

References

Audetat, A., Dolejs, D., Lowenstern, J.B., 2011. Molybdenite saturation in silicic magmas: occurrence and petrological implications. J. Petrol. 52 (5), 891–904.
Audetat, A., 2010. Source and evolution of molybdenum in the porphyry Mo(-Nb) deposit at Cave Peak, Texas. J. Petrol. 51 (8), 1739–1760.
Ballard, J.R., Palin, J.M., Williams, I.S., Campbell, I.H., 2001. Two ages of porphyry intrusion resolved for the super-giant Chuquicamata copper deposit of northern Chile by ELA-ICP-MS and SHRIMP. Geology 29 (5), 383–386.
Barra, F., Ruiz, J., Mathur, R., Titley, S., 2003. A Re–Os study of sulfide minerals from the Bagdad porphyry Cu–Mo deposit, northern Arizona, USA. Miner. Deposita 38, 585–596.
Barra, F., Ruiz, J., Valencia, V.A., Ochoa-Landín, Laramide, L., Chesley, J.T., Zurcher, L., 2005. Porphyry Cu–Mo mineralization in Northern Mexico: age constraints from Re-Os geochronology in molybdenite. Econ. Geol. 100, 1605–1616.
Bingen, B., Stein, H.J., 2003. Molybdenite Re-Os dating of biotite dehydration melting in the Rogaland high-temperature granulites, S Norway. Earth Planet. Sci. Lett. 208, 181–195.
Bookstrom, A.A., 1989. The Climax-Alma granite batholith of oligocene age and the porphyry molybdenum deposits of Climax, Colorado, USA. Eng. Geol. 27, 543–568.
Brooks, C.K., Tegner, C., Stein, H.J., Thomassen, B., 2004. Re-Os and $^{40}Ar/^{39}Ar$ ages of porphyry molybdenum deposits in the East Greenland volcanic-rifted margin. Econ. Geol. 99, 1215–1222.
Candela, P.A., Holland, H.D., 1986. A mass transfer model for copper and molybdenum in magmatic hydrothermal systems: the origin of porphyry-type ore deposits. Econ. Geol. 81, 1–19.
Carten, R.B., Geraghty, E.P., Walker, B.M., 1988. Cyclic development of igneous features and their relationship to high-temperature hydrothermal features in the Henderson porphyry molybdenum deposit, Colorado. Econ. Geol. 83, 266–296.
Carten, R.B., White, W.H., Stein, H.J., 1993. High-grade granite related molybdenum systems: classification and origin. In: Kirkham, R.V., Sinclair, W.D., Thorpe, R.I., Duke, J.M. (Eds.), Mineral Deposit Modeling, pp. 521–554. Geological Association of Canada Special Paper 40.
Chapin, C.E., 2012. Origin of the Colorado mineral belt. Geosphere 8 (1), 28–43.
Chiaradia, M., Schaltegger, U., Spikings, R., Wotzlaw, J.F., Ovtcharova, M., 2013. How accurately can we date the duration of magmatic-hydrothermal events in porphyry systems?—an invited paper. Econ. Geol. 108 (4), 565–584.
Chen, Z.G., Zhang, L.C., Wan, B., Wu, H.Y., Cleven, N., 2011. Geochronology and geochemistry of the Wunugetushan porphyry Cu–Mo deposit in NE China, and their geological significance. Ore Geol. Rev. 43, 92–105.
Cline, J.S., Bodnar, R.J., 1991. Can economic porphyry copper mineralization be generated by a typical calc-alkaline melt? J. Geophys. Res. 96 (B5), 8113–8126.
Cui, G., Wang, J.Y., Zhang, J.X., Cui, G., 2008. U-Pb SHRIMP dating of zircons from Duobaoshan granodiorite in Heilongjiang and its geological significance. Global Geol. 27 (14), 387–394 (in Chinese with English abstract).
Feely, M., Selby, D., Hunt, J., Conliffe, J., 2010. Long-lived granite-related molybdenite mineralization at Connemara, western Irish Caledonides. Geol. Mag. 147 (6), 886–894.
Fu, R.Z., Kan, X.S., Meng, Z.J., Wan, g J.P., 2011. Geological characteristics of Chalukou porphyry molybdenum polymetallic deposit, Daxinganling, Heilongjiang province. Mineral Explor. 2 (3), 232–240 (in Chinese with English abstract).
Gardien, V., Rabinowicz, M., Vigneresse, J., Dubois, M., Boulvais, P., Martini, R., 2016. Long-lived interaction between hydrothermal and magmatic fluids in the Soultz-sous-Forêts granitic system (Rhine Graben, France). Lithos 246–247, 110–127.
Ge, W.C., Lin, Q., Li, X.H., Wu, F.Y., Sun, D.Y., 2000. Geochemical characteristics of basalts of the Early Cretaceous Yiliekede formation, North Daxing'anling. J. Mineral. Petrol. 20 (3), 14–18 (in Chinese with English abstract).
Ge, W.C., Wu, F.Y., Zhou, C.Y., Rahman, A.A., 2005. Emplacement age of the Tahe granite and its constraints on the tectonic nature of the Erguna block in the northern part of the Da Hinggan Range. Chin. Sci. Bull. 50 (18), 2097–2105 (in Chinese).
Ge, W.C., Wu, F.Y., Zhou, C.Y., Zhang, J.H., 2007. Porphyry Cu–Mo deposits in the eastern Xing'an–Mongolian Orogenic Belt: mineralization ages and their geodynamic implications. Chin. Sci. Bull. 52, 3416–3427 (in Chinese).
Guo, F., Fan, W.M., Gao, X.F., Li, C.W., Miao, L.C., Zhao, L., Li, H.X., 2010. Sr–Nd–Pb isotope mapping of Mesozoic igneous rocks in NE China: constraints on tectonic framework and Phanerozoic crustal growth. Lithos 120, 563–578.
Halter, W.E., Pettke, T., Heinrich, C.A., 2002. The origin of Cu/Au ratios in porphyry-type ore deposits. Science 296, 1844–1846.
Harris, A.C., Dunlap, W., Reiners, P.W., Allen, C.M., Cooke, D.R., White, N.C., Campbell, I.H., Golding, S.D., 2008. Multimillion year thermal history of a porphyry copper deposit: application of U-Pb, $^{40}Ar/^{39}Ar$ and (U–Th)/He chronometers, Bajo de la Alumbrera copper–gold deposit, Argentina. Miner. Deposita 43, 295–314.
Hou, K.J., Li, Y.H., Tian, Y.Y., 2009. In situ U-Pb zircon-dating using laser ablation-multi ion counting-ICP-MS. Mineral Deposits 28 (4), 481–492 (in Chinese with English abstract).
Hu, X.L., Yao, S.Z., He, M.C., Ding, Z.J., Liu, M., Cui, Y.B., Shen, J., 2014. Sulfur and lead isotopic characteristics of Chalukou and Daheishan porphyry Mo deposits in northern segment of Da Hinggan Mountains. Mineral Deposits 33 (4), 776–784 (in Chinese with English abstract).
Jachon, S.E., Pearson, N.J., Griffin, W.L., BeLousova, E.A., 2004. The application of laser ablation-inductively coupled plasma-mass spectrometry (LA-ICP-MS) to in situ U-Pb zircon geochronology. Chem. Geol. 211, 47–69.
Jahn, B., Wu, F.Y., Chen, B., 2000. Massive granitoid generation in Central Asia: Nd isotope evidence and implication for continental growth in the Phanerozoic. Episodes 23 (2), 82–92.
Jahn, B.M., Wu, F.Y., Capdevila, R., Martineau, F., Zhao, Z.H., Wang, Y.X., 2001. Highly evolved juvenile granites with tetrad REE patterns: the Woduhe and Baerzhe granites from the Great Xing'an Mountains in NE China. Lithos 59, 171–198.
Jin, L.Y., Qin, K.Z., Li, G.M., Li, Z.Z., Song, G.X., Meng, Z.J., 2015. Trace element distribution in sulfides from the Chaluko porphyry Mo vein type Zn Pb system, northern Great Xing'an Range, China: implication exploration. Acta Petrologica Sinica 31 (8). 2417–243 (in Chinese with English abstract).
Jin, L.Y., Qin, K.Z., Meng, Z.J., Li, G.M., Song, G.X., Li, Z.Z., 2014. Features and occurrences of veins in Chalukou giant molybdenum-zinc-lead deposit, northern Da Hinggan Mountains, and their indications for mineralization. Mineral Deposits 33 (4), 742–760 (in Chinese with English abstract).
JMIC (Jinxin Mining Industry Company), 2011. The Exploratory Report of Chalukou Mo–Pb–Zn Polymetallic Deposit at the Songling District, Great Xing'an Range District, Heilongjiang Province, 223 pp. (in Chinese).
Keith, J.D., Shanks, W.C., Archibald, D.A., Farrar, E., 1986. Volcanic and intrusive history of the pine grove porphyry molybdenum system, Southwestern Utah. Econ. Geol. 81, 553–577.
Klemm, L.M., Pettke, T., Heinrich, C.A., 2008. Fluid and source magma evolution of the Questa porphyry Mo deposit, New Mexico, USA. Miner. Deposita 43, 533–552.
Lerchbaumer, L., Audétat, A., 2013. The metal content of silicate melts and aqueous fluids in subeconomically Mo mineralized granites: implications for porphyry Mo genesis. Econ. Geol. 108 (5), 987–1013.
Li, Z.Z., Li, G.M., Meng, Z.J., Qin, K.Z., Song, G.X., Jin, L.Y., Kan, X.S., Wang, J., Zhang, X. N., 2014. Petrofacies classification, characteristics and formation mechanism of breccias in the Chalukou giant molybdenum deposit of Da Hinggan Mountains. Mineral Deposits 33 (3), 607–624 (in Chinese with English abstract).
Lin, Q., Ge, W.C., Cao, L., Sun, D.Y., Lim, K.G., 2003. Geochemistry of Mesozoic volcanic rocks in Da Hinggan Ling: the bimodal volcanic rocks. Geochimica 32 (3), 208–222 (in Chinese with English abstract).
Lin, Q., Ge, W.C., Wu, F.Y., Sun, D.Y., Cao, L., 2004. Geochemistry of Mesozoic granites in Da Hinggan Ling ranges. Acta Petrologica Sinica 20 (3), 403–412 (in Chinese with English abstract).
Liu, J., Mao, J.W., Wu, G., Luo, D.F., Hu, Y.Q., Li, T.G., 2014. Fluid inclusions and H-O–S–Pb isotope systematics of the Chalukou giant porphyry Mo deposit, Heilongjiang Province, China. Ore Geol. Rev. 59, 83–96.
Liu, J., Mao, J.W., Wu, G., Luo, D.F., Hu, Y.Q., 2014. Zircon U-Pb and molybdenite Re–Os dating of the Chalukou porphyry Mo deposit in the northern Great Xing'an Range, China and its geological significance. J. Asian Earth Sci. 79, 696–709.
Liu, J., Mao, J.W., Wu, G., Luo, D.F., Wang, F., Zhou, Z.H., Hu, Y.Q., 2013. Zircon U-Pb dating for the magmatic rocks in the Chalukou Porphyry Mo deposit in the Northern Great Xing′An Range China and its geological significance. Acta Geologica Sinica 87 (2), 208–226 (in Chinese with English abstract).
Liu, J., Mao, J.W., Wu, G., Wang, F., Luo, D.F., Hu, Y.Q., 2015. Geochemical signature of the granitoids in the Chalukou giant porphyry Mo deposit in the Heilongjiang Province, NE China. Ore Geol. Rev. 64, 35–52.
Liu, Y., Jiang, S., Bagas, L., 2016. The genesis of metal zonation in the Weilasituo and Bairendaba Ag–Zn–Pb–Cu–(Sn–W) deposits in the shallow part of a porphyry Sn–W–Rb system, Inner Mongolia, China. Ore Geol. Rev. 75, 150–173.
Liu, Y.F., Nie, F.J., Jiang, S.H., Xi, Z., Zhang, Z.G., Xiao, W., Zhang, K., Liu, Y., 2012. Ore-forming granites from Chaganhua molybdenum deposit, Central Inner Mongolia, China: Geochemistry, geochronology and petrogenesis. Acta Petrologica Sinica 28 (2), 409–420 (in Chinese with English abstract).
Liu, Y.F., Nie, F.J., Sun, Z.J., Lü, K.P., Zhang, K., Liu, Y., 2011. Discovery of Chalukou super-large-scale molybdenum polymetallic deposit, Northern Daxing'anlin Mountain, China, and its significance. Mineral Deposits 30 (4), 759–764 (in Chinese with English abstract).
Liu, Y.S., Gao, S., Hu, Z.C., Gao, C.G., Zong, K.Q., Wang, D.B., 2010. Continental and oceanic crust recycling-induced melt-peridotite interactions in the Trans-North China Orogen: U-Pb dating, Hf isotopes and trace elements in zircons from mantle xenoliths. J. Petrol. 51, 537–571 (in Chinese with English abstract).
Lowenstern, J.B., 1994. Dissolved volatile concentrations in an ore-forming magma. Geology 22, 893–896.
Lowenstern, J.B., Mahood, G.A., Hervig, R.L., Sparks, J., 1993. The occurrence and distribution of Mo and molybdenite in unaltered peralkaline rhyolites from Pantelleria, Italy. Contrib. Miner. Petrol. 114, 119–129.
Lü, K.P., Hang, L., Zhang, J.N., 2010. Geological features and prospecting marks of Chalukou porphyry deposit. Heilongjiang Sci. Technol. Inf. 21. 31–31 (in Chinese).

Lü, Z.C., Zhang, P.P., Liu, C.Q., Liu, J.J., 2000. Mineralogical characteristics of silver minerals in E'rentaolegai silver deposit. Geology - Geochemistry 28 (3), 41–47 (in Chinese with English abstract).
Ludington, S. Plumlee, S., 2009. Climax-Type Porphyry Molybdenum Deposits. Geological survey open-file report 2009–1215, 16pp.
Ludington, S., Hammarstrom, J., Piatak, N., 2009. Low-fluorine stockwork molybdenite deposits. U.S. Geological Survey open-file report 2009–1211, 9p.
Ludwig, K.R., 2003. ISOPLOT 3.00: A Geochronological Toolkit for Microsoft Excel, Berkeley Geochronology Center. Special Publication No. 4.
McCandless, T.E., Ruiz, J., 1993. Rhenium-osmium evidence for regional mineralization in Southwestern North America. Science 261, 1282–1286.
Meng, Q.R., 2003. What drove late Mesozoic extension of the northern China-Mongolia tract? Tectonophysics 369, 155–174.
Miao, L.C., Liu, D.Y., Zhang, F.Q., Fan, W., Shi, Y.R., Xie, H.Q., 2007. Zircon SHRIMP U-Pb ages of the "Xinghuadukou Group" in Hanjiayuanzi and Xinlin areas and the "Zhalantun Group" in Inner Mongolia, Da Hinggan Mountains. Chi. Sci. Bull. 52 (8), 1112–1124.
Mutschler, F., Wright, E., Ludington, S., Abbott, J., 1981. Granite molybdenite systems. Econ. Geol. 76 (4), 874–897.
Nasdala, L., Hofmeister, W., Norberg, N., Mattinson, J.M., Corfu, F., Drr, W., Kamo, S. L., Kennedy, A.K., Kronz, A., Reiners, P.W., Frei, D., Kosler, J., Wan, Y., Gtze, J., Hger, T., Krner, A., Valley, J., 2008. Zircon M257 - a homogeneous natural reference material for the ion microprobe U-Pb analysis of zircon. Geostand. Geoanal. Res. 32, 247–265.
Nie, F.J., Jiang, S.H., 2011. Geological setting and origin of Mo–W–Cu deposits in the Honggor-Shamai District, Inner Mongolia, North China. Resource Geol. 61 (4), 344–355 (in Chinese).
Nie, F.J., Sun, Z.J., Li, C., Liu, Y.F., Lü, K.P., Zhang, K., Liu, Y., 2011. Re-Os isotopic dating of molybdenite separates from Chalukou porphyry Mo polymetallic deposit in Heilongjiang Province. Mineral Deposits 30 (5), 828–836 (in Chinese with English abstract).
Pettke, T., Oberli, F., Heinrich, C.A., 2010. The magma and metal source of giant porphyry-type ore deposits, based on lead isotope microanalysis of individual fluid inclusions. Earth Planet. Sci. Lett. 296, 267–277.
Pirajno, F., Zhou, T.F., 2015. Intracontinental Porphyry and Porphyry-Skarn mineral systems in Eastern China: scrutiny of a special case "Made-in-China". Econ. Geol. 110 (3), 603–629.
Qin, K.Z., Li, H.M., Li, W.S., 1999. Intrusion and mineralization ages of Wunugetushan porphyry Cu-Mo deposit, Inner Mongolia, Northeastern China. Geol. Rev. 45 (2), 180–185 (in Chinese with English abstract).
Quadt, A.V., 2011. Zircon crystallization and the lifetimes of ore-forming magmatic-hydrothermal systems. Geology 39 (8), 731–734.
Schönwandt, H.K., Petersen, J.S., 1983. Continental riffing and porphyry-molybdenum occurrences in the Oslo region, Norway. Tectonophysics 94, 609–631.
Shao, J.A., Zhang, L.Q., Mu, B.L., 1999. Magmatism in the Mesozoic extending orogenic process of Da Hinggan MTS. Earth Sci. Front. 6 (4), 339–346 (in Chinese with English abstract).
Shinohara, H., Kazahaya, K., Lowenstern, J.B., 1995. Volatile transport in a convecting magma column: implications for porphyry Mo mineralization. Geology 23 (12), 1091–1094.
Sillitoe, R.H., Mortensen, J.K., 2010. Longevity of porphyry copper formation at Quellaveco, Peru. Econ. Geol. 105, 1157–1162.
Sláma, J., Kosler, J., Condon, D.J., Crowley, J.L., Gerdes, A., Hanchar, J.M., Horstwood, M.S.A., Morris, G.A., Nasdala, L., Norberg, N., Schaltegger, U., Schoene, B., Tubrett, M.N., Whitehouse, M.J., 2008. Plesovice zircon — a new natural reference material for U-Pb and Hf isotopic microanalysis. Chem. Geol. 249, 1–35.
Sun, L.X., Ren, B.F., Zhao, F.Q., Ji, S.P., Geng, J.Z., 2013. Late Paleoproterozoic magmatic records in the Eerguna massif: evidence from the zircon U-Pb dating of granitic gneisses. Geol. Bull. China 32 (2–3), 341–352.
Tomurtogoo, O., Windley, B.F., Kroner, A., Badarch, G., Liu, Y.D., 2005. Zircon age and occurrence of the Adaatsag ophiolite and Muron shear zone, central Mongolia: constraints on the evolution of the Mongol-Okhotsk ocean, suture and orogen. J. Geol. Soc. 162, 125–134.
Villeneuve, M., Whalen, J.B., Anderson, R.G., Struik, L.C., 2001. The Endako Batholith: episodic plutonism culminating in formation of the Endako porphyry molybdenite deposit, North-Central British Columbia. Econ. Geol. 96 (1), 171–196.
Wallace, S.R., MacKenzie, W.B., Blair, R.G., Muncaster, N.K., 1978. Geology of the Urad and Henderson molybdenite deposits, Clear Creek County, Colorado, with a section on a comparison of these deposits with those at clinlax, Colorado. Econ. Geol. 73, 325–368.
Wang, J.P., Han, L., Lü, K.P., 2011. Geological characteristics the Chalukou molybdenum polymetallic ore deposit, Daxing'anling. Resour. Geol. 25 (6), 486–490 (in Chinese with English abstract).
Westra, G., Keith, S., 1981. Classification and genesis of stockwork molybdenum deposits. Econ. Geol. 76 (4), 844–873.
White, W.H., Bookstrom, A.A., Kamilli, R.J., Ganster, M.W., Smith, R.P., Ranta, D.E., Steininger, R.C., 1981. Character and origin of climax-type molybdenum deposits. Econ. Geol. 75th Anniversary Volume, 270–316.
Wu, F.Y., Jahn, B.M., Wilde, S., Lo, C.H., Yu, T.F., Lin, Q., Ge, W.C., Sun, D.Y., 2003. Highly fractionated I-type granites in NE China (II): isotopic geochemistry and implications for crustal growth in the Phanerozoic. Lithos 67, 191–204.
Wu, F.Y., Jahn, B.M., Wilde, S.A., Lo, C.H., Yui, T.F., Lin, Q., Ge, W.C., Sun, D.Y., 2003. Highly fractionated I-type granites in NE China (I): geochronology and petrogenesis. Lithos 66, 241–273.
Wu, F.Y., Sun, D.Y., Ge, W.C., Zhang, Y.B., Grant, M.L., Wilde, S.A., Jahn, B.M., 2011. Geochronology of the Phanerozoic granitoids in northeastern China. J. Asian Earth Sci. 41, 1–30.
Wu, F.Y., Sun, D.Y., Li, H.M., Jahn, B.M., Wilde, S., 2002. A-type granites in northeastern China, age and geochemical constraints on their petrogenesis. Chem. Geol. 187, 143–173.
Wu, F.Y., Sun, D.Y., Lin, Q., 1999. Petrogenesis of the Phanerozoic granites and crustal growth in Northeast China. Acta Petrologica Sinica 15 (2), 181–189 (in Chinese with English abstract).
Wu, G., Sun, F.Y., Zhu, Q., Li, Z.T., Ding, Q.F., Li, G.Y., Pang, Q.B., Wang, H.B., 2006. Geological characteristics and genesis of gold deposits in Upper Heilongjiang Basin. Mineral Deposits 25 (3), 215–230 (in Chinese with English abstract).
Wu, G., Chen, Y.C., Chen, Y.J., Zeng, Q.T., 2012. Zircon U-Pb ages of the metamorphic supracrustal rocks of the Xinghuadukou Group and granitic complexes in the Argun massif of the northern Great Hinggan Range, NE China, and their tectonic implications. J. Asian Earth Sci. 49, 214–233.
Wu, G., Chen, Y.C., Sun, F.Y., Liu, J., Wang, G.R., Xu, B., 2015. Geochronology, geochemistry, and Sr–Nd–Hf isotopes of the early Paleozoic igneous rocks in the Duobaoshan area, NE China, and their geological significance. J. Asian Earth Sci. 97, 229–250.
Xiang, A.P., Wang, Y.J., Qin, D.J., She, H.Q., Han, Z.G., Guan, J.D., Kang, Y.J., 2014. Metallogenic and diagenetic age of Honghuaerji tungsten polymetallic deposit in Inner Mongolia. Mineral Deposits 33 (2), 428–439 (in Chinese with English abstract).
Xiao, W.J., Windley, B.F., Hao, J., Zhai, M.G., 2003. Accretion leading to collision and the Permian Solonker suture, Inner Mongolia, China: termination of the central Asian orogenic belt. Tectonics 22, 1484–1505.
Xie, C.B., Liu, M., 2001. Geological features and genetic type of Chaganbulagen Ag, Pb, Zn (Au) deposit. World Geol. 20 (1), 25–29 (in Chinese with English abstract).
Xiong, S.F., He, M.C., Yao, S.Z., Cui, Y.B., Hu, X.L., Chen, B., 2014. Compositions and microthermometry of fluid inclusions of the Chalukou porphyry Mo deposit from Great Xing'an Range: implications for ore genesis. Earth Sci. (Journal of China University of Geosciences) 39 (7). 820–636 (in Chinese with English abstract).
Xu, D.Q., Nie, F.J., Jiang, S.H., Zhang, W.Y., Yun, F., Yang, C., Zhang, T.J., Lǔ, X.G., Lin, R. L., 2008. Geological and geochemical characteristics of the Aobaotu fluorite deposit in Inner Mongolia. Acta Geoscientica Sinica 29 (4), 440–450 (in Chinese with English abstract).
Xu, B., Zhao, P., Bao, Q.Z., Zhou, Y.H., Wang, Y.Y., Luo, Z.W., 2014. Preliminary study on the pre-Mesozoic tectonic unit division of the Xing-Meng Orogenic Belt (XMOB). Acta Petrologica Sinica 30 (7), 1841–1857 (in Chinese with English abstract).
Xu, B., Zhao, P., Wang, Y.Y., Liao, W., Luo, Z.W., Bao, Q.Z., Zhou, Y.H., 2015. The pre-Devonian tectonic framework of Xing'an–Mongolia orogenic belt (XMOB) in north China. J. Asian Earth Sci. 97, 183–196.
Xu, W.L., Wang, F., Pei, F.P., Meng, E., Tang, J., Xu, M.J., Wang, W., 2013. Mesozoic tectonic regimes and regional ore-forming background in NE China: constraints from spatial and temporal variations of Mesozoic volcanic rock associations. Acta Petrologica Sinica 29 (2), 339–353 (In Chinese with English abstract).
Yang, M.C., Liu, Y.J., Han, G.Q., Wang, C.B., Wen, Q.B., Zhao, Y.L., Liang, C.Y., Mi, X.N., 2011. Provenance analysis and its tectonic significance of Lower Carboniferous Hongshuiquan Formation sandstone in Yimin area of Inner Mongolia. Global Geol. 30 (2), 192–207 (in Chinese with English abstract).
Ying, J.F., Zhou, X.H., Zhang, L.C., Wang, F., Zhang, Y.T., 2010. Geochronological and geochemical investigation of the late Mesozoic volcanic rocks from the Northern Great Xing'an Range and their tectonic implications. Int. J. Earth Sci. 99, 357–378.
Zhang, C., Li, N., 2017. Geochronology and zircon Hf isotope geochemistry of granites in the giant Chalukou Mo deposit, NE China: implications for tectonic setting. Ore Geol. Rev. 81, 780–793.
Zhang, L.C., Chen, Z.G., Zhou, X.H., Ying, J.F., Wang, F., Zhang, Y.T., 2007. Characteristics of deep sources and tectonic-magmatic evolution of the early Cretaceous volcanics in Genhe area, Da-Hinggan Mountains: constraints of Sr-Nd-Pb-Hf isotopic geochemistry. Acta Petrologica Sinica 23 (11), 2823–2835 (in Chinese with English abstract).
Zhao, Y.M., Bi, C.S., Zou, X.Q., Sun, Y.L., Du, A.D., Zhao, Y.M., 1997. The Re-Os isotopic age of molybdenite from Duobaoshan and Tongshan porphyry copper (molybdenum) deposits. Acta Geoscientia Sinica 18 (1), 61–67 (in Chinese with English abstract).
Zhao, Z., Chi, X.G., Pan, S.Y., Liu, J.F., Sun, W., Hu, Z.C., 2010. Zircon U-Pb LA-ICP-MS dating of Carboniferous volcanics and its geological significance in the northwestern Lesser Xing' an Range. Acta Petrologica Sinica 26 (8), 2452–2464 (in Chinese with English abstract).
Zhao, Z., Chi, X.G., Zhao, X.Y., Sun, W., Pan, S.Y., Hu, Z.C., 2012. LA-ICP-MS U-Pb geochronology of detrital zircon from the Hongshui-quan formation in the Northern Da Hinggan area and its tectonic significance. J. Jilin Univ. (Earth Science Edition) 42 (1), 126–135 (in Chinese with English abstract).
Zhou, J.B., Wilde, S.A., Zhang, X.Z., Zhao, G.C., Liu, F.L., Qiao, D.W., Ren, S.M., Liu, J.H., 2011. A >1300 km late Pan-African metamorphic belt in NE China: new evidence from the Xing'an block and its tectonic implications. Tectonophysics 509, 280–292.
Zhou, Z.H., Mao, J.W., Lyckberg, P., 2012. Geochronology and isotopic geochemistry of the A-type granites from the Huanggang Sn–Fe deposit, southern Great Hinggan Range, NE China: implication for their origin and tectonic setting. J. Asian Earth Sci. 49, 272–286.